Tracking and Pair Dispersion Analysis of Buoyant Particles in a Turbulent Shear Flow

Stephanie Paustian

A thesis submitted in partial fulfillment
of the requirements for the degree of

Master of Science in Mechanical Engineering

University of Washington

2015

Committee:

Alberto Aliseda

John Kramlich

Brian Polagye

Alex Horner-Devine

Program Authorized to Offer Degree:

Mechanical Engineering

University of Washington

Abstract

Tracking and Pair Dispersion Analysis of Buoyant Particles in a Turbulent Shear Flow

Stephanie Paustian

Chair of the Supervisory Committee:
Associate Professor Alberto Aliseda
Mechanical Engineering

Presented are experimental measurements of one and two-particle dispersion in a turbulent shear flow. The baseline flow is a well-characterized high Reynolds number turbulent submerged round jet. Buoyant air bubbles and canola oil droplets were injected into the jet within the self-similar region at five injection locations and five jet Reynolds numbers ranging from 18,000 to 34,000. Images of two particles, injected simultaneously, were obtained from high-speed shadowgraphy. The particles were then tracked using a four-frame predictive algorithm. The influence of mean shear and turbulent fluctuations on dispersion is analyzed for initial positions where a mean velocity shear is superimposed on turbulent fluctuations. The results were analyzed to determine the influence of the density ratio, the non-dimensional shear rate, Reynolds number, and the turbulence intensity (these last three associated with the location of injection) on single-particle and two-particle dispersion.

Table of Contents

List of Figures

List of Tables

Acknowledgments

I am very grateful to my advisor, Professor Alberto Aliseda, who provided excellent guidance and unyielding encouragement throughout all of my endeavors at the University of Washington. This work would not have been possible without the support of the members of the Cardiovascular and Multiphase Flow Lab, as well as the faculty and staff members of the University of Washington Mechanical Engineering Department. Last, I would like to thank my family and friends for their unwavering support and for always encouraging me to challenge myself.

Chapter 1: Introduction

One of turbulence's most prominent features is the ability to distribute transportable quantities throughout a flow and, together with molecular diffusion, ultimately leads to mixing. This ability to disperse fluid particles to all regions of the flow can be understood and modeled by examining the evolution within the flow of the relative separation of two particles injected at a small distance from each other, i.e. pair dispersion. Similarly, single particle dispersion, the evolution of the distance that a particle travels from its source famously studied by G.I. Taylor in 1921 [1]. Both single particle and pair dispersion allow us to understand the process by which turbulence moves two fluid particles that were originally very close to each other, and thus had very similar properties (chemical composition, momentum, vorticity, energy, etc.), towards widely different positions. As the two particles move apart, they will have an increasing tendency to mix with the ambient (fluid particles with different properties) since both the difference in fluid property values between the particle and the environment (the gradient), and the amount of contact area between the particle and the surrounding fluid will be enhanced. In the same way that the statistics of the distance that one particle from its original position is displaced by the turbulent flow gives us a way to estimate the spatial reach of fluid injected at a source, two-particle dispersion gives us a measure of the separation between particles that start very close to each other (or the "closeness" between particles that started out far from each other, if we reverse time) due to the turbulent stirring at different scales [2]. Examining how a pair of particles disperse in a flow as time evolves, teaches us how the different scales of turbulence interact with the pair as their distance increases and how the turbulent kinetic energy, distributed through a wide spectrum of spatial and temporal scales results into stirring and mixing fluids.

1.1 Single Particle Dispersion of Fluid Tracers

Before tackling the problem of two-particle dispersion, we will first examine turbulent single-particle dispersion. This problem, pioneered by Richardson and Taylor in the early 20th century [3] [1] has been studied primarily in homogeneous, isotropic turbulence. In this type of flow, the position of a particle relative to its initial position is controlled only by the turbulent velocity fluctuations, which are the same in all directions. In the absence of a mean flow, particles are transported by turbulent eddies.

In 1921, Taylor developed a theory to predict this behavior, in the famously titled "Diffusion by Continuous Movements" paper. His analysis reduces the problem of single particle dispersion to that of determining the autocorrelation function (R_ξ). The result relates the mean square of the particle's displacement to the mean square of the fluid velocity fluctuations and to the correlation coefficient relating the velocity of the fluid particle at times t and t+ξ [1].

$$[X^2] = 2[u^2] \int_0^T \int_0^t R_\xi d\xi dt \tag{1}$$

$$R_\xi = \frac{[u(t)u(t+\xi)]}{[u^2(t)]} \tag{2}$$

This result can be simplified for different time scales. For very small times, when R_ξ can be considered to be approximately unity, equation 1 becomes [1]:

$$[X^2(t)] = [u^2]t^2 \tag{3}$$

Over a large interval of time, when the final velocity of the particle has no correlation to the initial velocity, the mean square of the position is expected to increase linearly with time. As shown in the following equation, where *I* is the integral time scale.

$$[X^2(t)] = 2I[u^2]t \tag{4}$$

While this result has been very influential on the study of turbulent diffusion, it is only fully applicable under very specific conditions. Equation 1 relies on the existence of homogeneous isotropic flow, which is a highly idealized flow field that does not accurately represent the conditions of most mixing applications. Additionally, it describes the behavior of fluid tracers and, therefore, produces increasing errors in the effort to model the dispersion of particulate matter in the flow as the particle's properties increasingly differ from those of the fluid.

1.2 Single Particle Dispersion of Inertial Particles

Although it is important to understand how fluid tracers act within a flow, the dynamics of inertial particles hold the key to understanding many of the open questions in turbulent multiphase flows, and to solving many significant applications. Understanding the dispersion of inertial particles allows for modeling of sediment in waterways and particulate matter or water droplets in the atmosphere. A seminal study of the effects of inertial particles on single particle dispersion was published in 1971 by

Snyder and Lumley [4]. In it, the dispersion of particles in a wind tunnel with grid turbulence was characterized. The particles studied had widely different densities, and satisfy the condition of being smaller than the Kolmogorov length scale (on the order of 10%). The mean square of the dispersion obtained in those experiments can be seen in Figure 1 below.

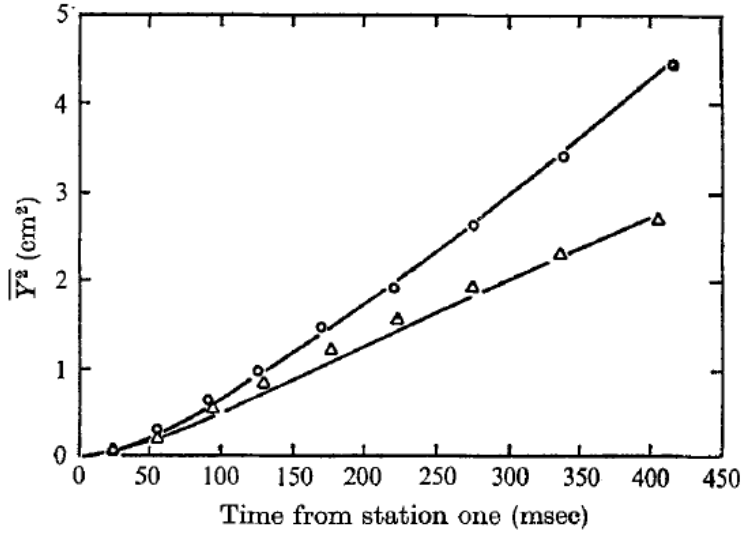

Figure 1: Experimental results of single particle dispersion of inertial particles [3]. Circles represent glass particles (density of 260 kg/m^3) and triangles are for corn pollen (density of 1000 kg/m^3).

The results of the measurements correspond very closely with the values predicted from the double integration of the autocorrelation function predicted by Taylor. The results show that heavier particles have hindered dispersion due to the turbulence. It was hypothesized that the dispersion of particles with higher inertia is influenced by the crossing-trajectories effect. Under the effect of gravity, particles have a velocity relative to the fluid (crossing the fluid trajectories), so they effectively tumble from one eddy to another, partially canceling their effect on dispersion, whereas fluid tracers would remain in the same eddy for the entire lifetime of that eddy. Wells and Stock [5] confirmed this hypothesis by careful experiments in which water droplets charged electrically at injection where subject to increasing electric fields opposing gravity, as they dispersed in a horizontal wind tunnel with grid turbulence. By partially cancelling the crossing trajectories effect due to gravity, it was shown that this effect indeed was responsible for the hindered dispersion of heavy particles.

1.3 Two-Particle Dispersion of Fluid Tracers

Two-particle dispersion characterizes the effect of turbulence on the particles, passive tracers or inertial particles, by computing the separation between particle pairs that are injected in the flow at different positions, simultaneously, or at different times, from the same position. The coupled effect of turbulence on each of the particles, due to the velocity correlation at the particles locations, from small and large scales is differentiated from their displacements from their original injection position. That is to say, the statistics of the particle pair separation differ from the statistics of each particle's displacement added together (in vector form, and then its norm as the distance between particles) because the two particles do not move in an uncorrelated field of velocity fluctuations but rather in a flow where the cross-correlation between the velocities at two points depends strongly on the separation between those points (as represented by the spectrum of turbulent kinetic energy).

One important consideration for analysis of two-particle dispersion is the initial separation of the particles. In homogeneous, isotropic flow, particles are dispersed most quickly by eddies whose size is approximately equal to the distance between the particles. This is because when the size of the eddy is much larger than the distance between the particles it causes the particles to drift in the same direction as opposed to move apart, and when the size of the eddy is much smaller than the distance between the particles it will not contain enough energy to have a perceptible effect on the separation. Therefore, the initial separation of the particles indicates the size of eddies responsible for their initial dispersion. As the particles continue to disperse, their separation is affected by larger and larger eddies, effectively increasing the relative velocity between them. Batchelor showed in 1950 that, for an initial separation in the inertial subrange $\left(\left(\frac{\nu^3}{\varepsilon}\right)^{1/4} < \Delta_0 < \frac{u\prime^3}{\varepsilon}\right)$, the mean square of the separation for short times can be described by equation 5, where C is the universal Kolmogorov's constant in the inertial range scaling law, equal to 2.13, and ε is the local energy dissipation rate of the flow [2].

$$[\,(\Delta(t) - \Delta_0)^2\,] = \frac{11}{3} C(\varepsilon \Delta_0)^2 t^2 \tag{5}$$

$$\text{For } t < t_0 = \left(\frac{\Delta_0^2}{\varepsilon}\right)^{1/3}$$

The time over which this equation is appropriate is the characteristic time scale during which the fluid elements will "remember" their initial relative velocity. After this time, the initial eddy responsible for

the particle pair separation will break up and the particles will have moved to a larger separation, being influenced by increasingly higher energy, larger, eddies.

Bourgoin et. al. [6] tested Batchelor's hypothesis studying the pair dispersion of tracer particles in approximately homogeneous, isotropic turbulence through 3D particle tracking. They found that for a very wide range of initial separations, their data followed the predicted t^2 scaling. Figure 2 below shows the results of this research, comparing data scaled by the constant $(11c/3)(\varepsilon\Delta_0)^{2/3}$ to equation 5, represented by the black solid line. The inset within the figure shows the curves scaled by the Kolmogorov time scale which do not collapse as well, showing that t_0 is the characteristic time for the initial t-squared dispersion regime.

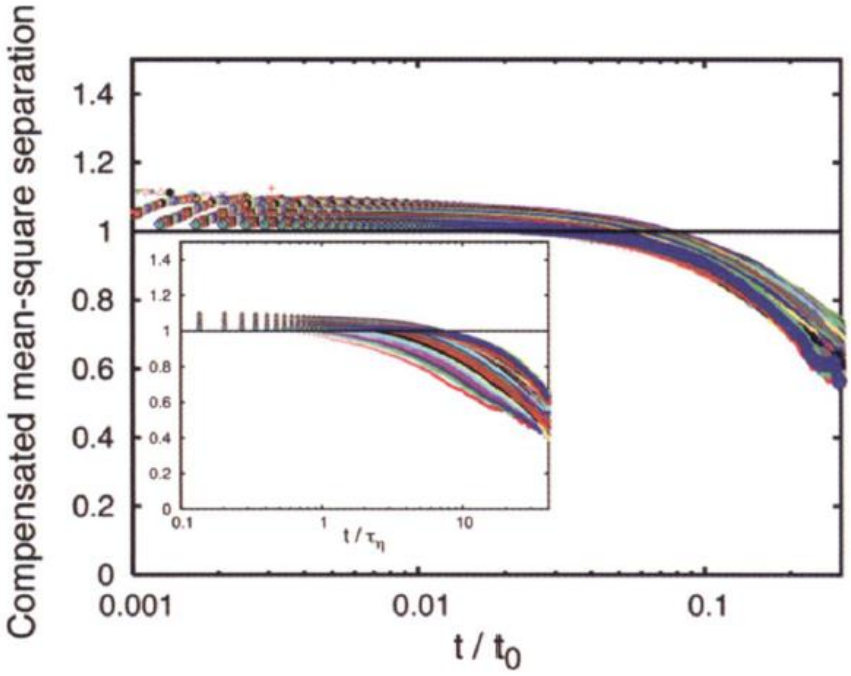

Figure 2: Experimental comparison of two-particle dispersion to Batchelor's t^2 law [4]

Similarly to the equation for single particle dispersion given in section 1.1, equation 5 only applies to the pair dispersion of fluid tracers in homogeneous, isotropic turbulence. Further studies are needed to determine the validity of Batchelor's law in the prediction of pair dispersion for inertial or buoyant particles, and in non-homogeneous, sheared flows.

For times on the order of the characteristic time, t_0, pair dispersion is predicted to transition into Richardson-Obukhov scaling [3] [6]. In this super-diffusive regime, the mean square of the separation

between the particles is predicted to scale with t^3. Richardson predicted that the diffusion can be described as [7]:

$$[\,\Delta(t)^2\,] = g\varepsilon t^3 \tag{6}$$

where ε is the turbulent energy dissipation rate and g is a universal constant, equal to 0.5 [7]. Jullien et. al. [7] tested this theory in 1999 and observed t^3 scaling in the separations of simulated particle pairs in two-dimensional turbulence, based on velocity fields measured by PIV techniques. Their results can be seen in Figure 3.

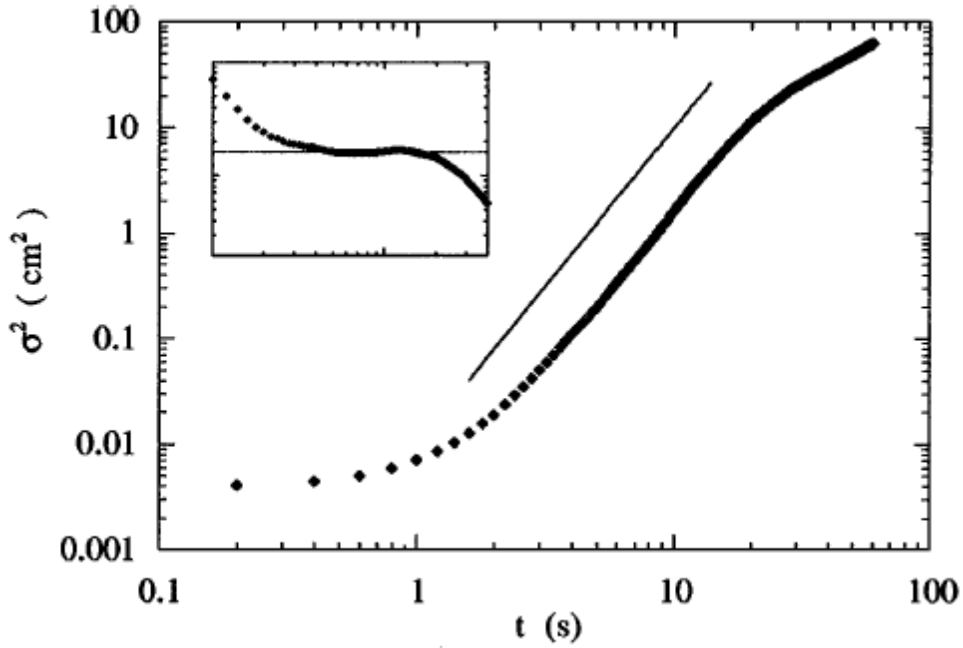

Figure 3: Mean squared separation of 10^4 particles. Inset: curve divided by t^3 [7]

1.4 Two-Particle Dispersion of Inertial Particles

Gibert et. al. [8] recently published a study on the effects of particle inertia on two-particle dispersion. The study was carried out in a turbulence box (or Von Karman) flow that contained a small region of approximately isotropic and homogeneous turbulence, with negligible mean flow. The particles had sizes comparable to the Kolmogorov scale with densities ranging from neutrally buoyant ($\rho_p/\rho_f \approx 1$) to inertial ($\rho_p/\rho_f \approx 8$). Heavy particles were observed to disperse faster than neutrally-buoyant particles with the same initial separations, as can be seen in Figure 4 below. The data is again normalized by

Batchelor's predictions. Similarly to the experiment mentioned in section 1.3, the tracer particles follow the predicted path for short times, and start deviating from the t^2 law at 0.01 times the eddy turn over time based on the initial separation. This experiment showed that the inertial particles initially separated faster than the tracer particles. While these observations shed some light on the interactions of particles with turbulent flows, many questions still remain on the behavior of particles in more complex flows.

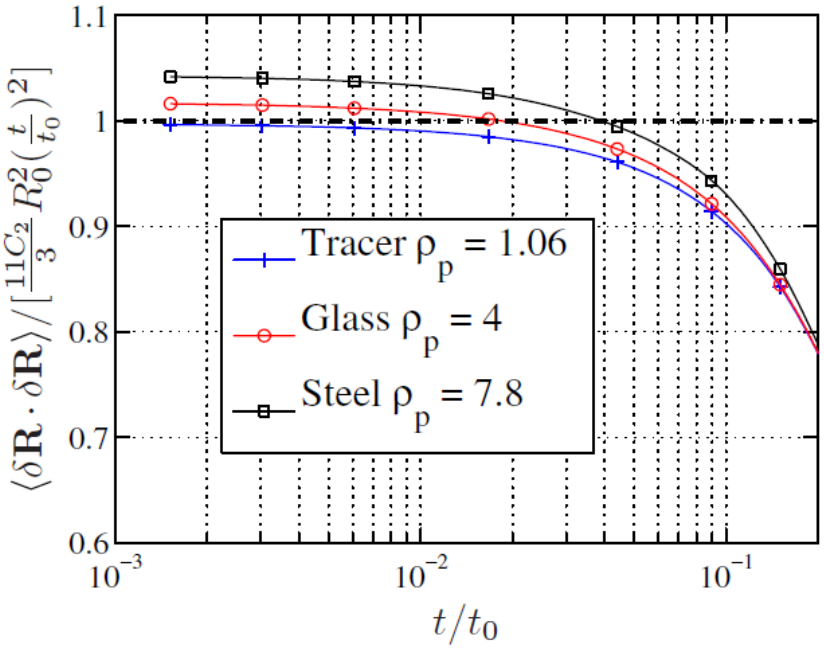

Figure 4: Experimental comparison of inertial particles to two-particle dispersion equation [8]

1.5 Turbulent Round Jets

A round free jet is a conical flow produced when fluid issues through a round nozzle into an infinite, quiescent surrounding fluid. As the high momentum fluid crosses from the nozzle exit and is exposed to the initially stagnant fluid, its starts to entrain the surrounding fluid, mixing the high and zero momentum fluids, and shedding vortices as a result of the Kelvin-Helmholtz instability that develop at the interface between the two fluids. As a result of these processes, the jet spreads forming a mean interface with an axisymmetric conical shape at a constant 13.5-degree half angle.

1.5.1 Velocity Field

The dominant component of the mean velocity of a turbulent jet is in the axial direction. This velocity decreases with height above the nozzle and with radial distance from the centerline as shown in Figure 5. After an initial development region, the potential cone, the mean flow is well represented by a self-similar solution based on the conservation of momentum in the jet and the lack of a characteristic length (no confinement). The mean centerline velocity, which is a function of distance downstream x, can be calculated as shown in equation 7 [9].

$$U_c(x) = \frac{U_j * B * d}{x - x_o} \tag{7}$$

In this equation, U_J is the jet velocity at the nozzle, B is an empirical constant equal to 5.8, d is the diameter of the nozzle, x is the downstream distance from the nozzle, and x_0 is a virtual origin necessary to match the self-similar solution to the real jet, in which the velocity evolves in the development region and is not U_J at x=0. The virtual origin of the jet is calculated by determining the x-intercept of the line formed by plotting $U_J/U_0(x)$ as a function of x/d. For the jet used in this study, the virtual origin is located at $x_0/d = 4$.

The radial dependency of the jet axial velocity is Gaussian, spreading with distance from the axis. Because the axial velocity does not decay to zero with radial distance, except as it tends to infinity, the width of the jet is not clearly defined. To give an unequivocal definition of the jet width, the radial distance where the mean velocity is equal to ½ the centerline mean velocity, at any given distance downstream of the nozzle, is defined as the jet half-width. The spreading of the jet can be shown as an increase in the half-width of the jet with distance from the nozzle. The half-width of the jet can be calculated as:

$$r_{1/2}(x) = S(x - x_0) \tag{8}$$

where S is the spreading rate of the jet, and has been experimentally determined to be 0.094 corresponding to the tan(13.5°) for a turbulent round free jet [9].

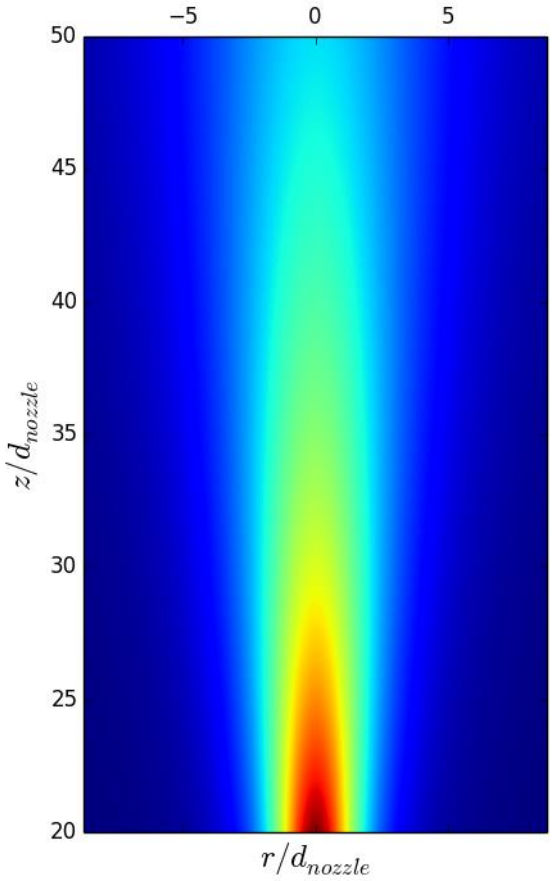

Figure 5: Axial velocity of a turbulent round jet

1.5.2 Turbulence Dissipation Rate

Turbulent motion is characterized by a collection of eddies of various sizes. The large eddies of turbulent motion are gradually broken up into smaller and smaller eddies, passing along their kinetic energy. As eddies decrease in size, their movement is more influenced by viscosity until eventually, at the smallest scales, all the kinetic energy of the fluid fluctuations is converted into internal energy by viscous dissipation. The rate at which the energy is transferred across scales from the largest to the smallest is constant for a wide range, the inertial range, where the Reynolds number of the turbulent eddies is large. This constant, characteristic of the turbulence is called the turbulence dissipation rate (ε). For the turbulent round free jet, an empirical correlation for the turbulence dissipation rate (per unit mass) is given by equation 9 [10]:

$$\frac{2\varepsilon(x-x_0)}{U_c^3} = [0.3549 + 11.99\eta^2 - 1635\eta^4 + 43470\eta^6]e^{-201\eta^2} \quad (9)$$

where η is the nondimensional position, defined as $\eta = r/(x-x_0)$. The result of equation 9 can be seen in Figure 6.

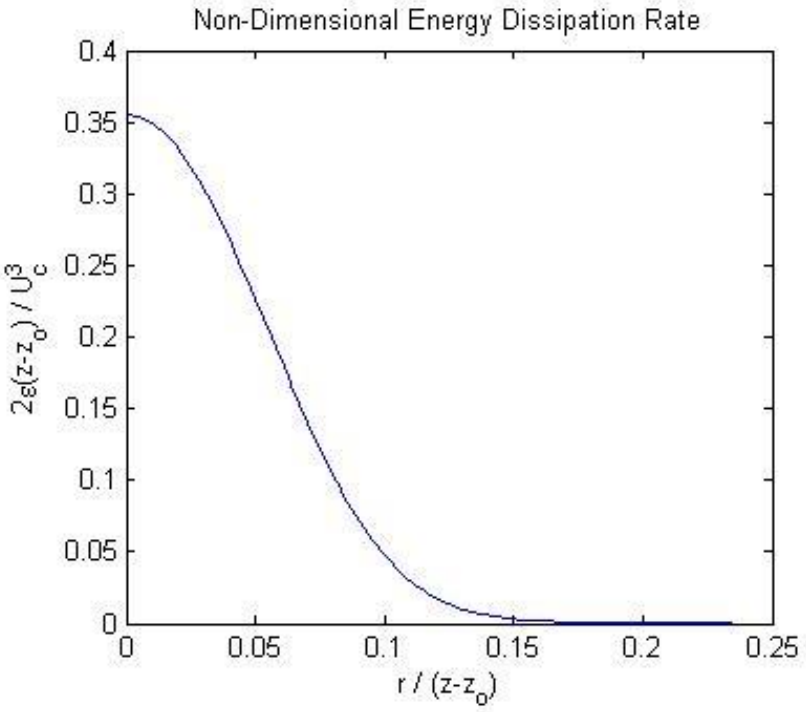

Figure 6: Non-dimensional energy dissipation rate per unit mass

The energy dissipation rate decreases with vertical distance from the nozzle and radial distance from the centerline as shown in Figure 7. The equations from the previous sections describing single particle and pair dispersion for homogeneous flow predict that the mean square of the dispersion increases with the energy dissipation rate. The spatially changing dissipation rate within the jet will therefore result in deviations from the dispersion values predicted for homogeneous, isotropic flows because the energy dissipation rate changes with position within the jet.

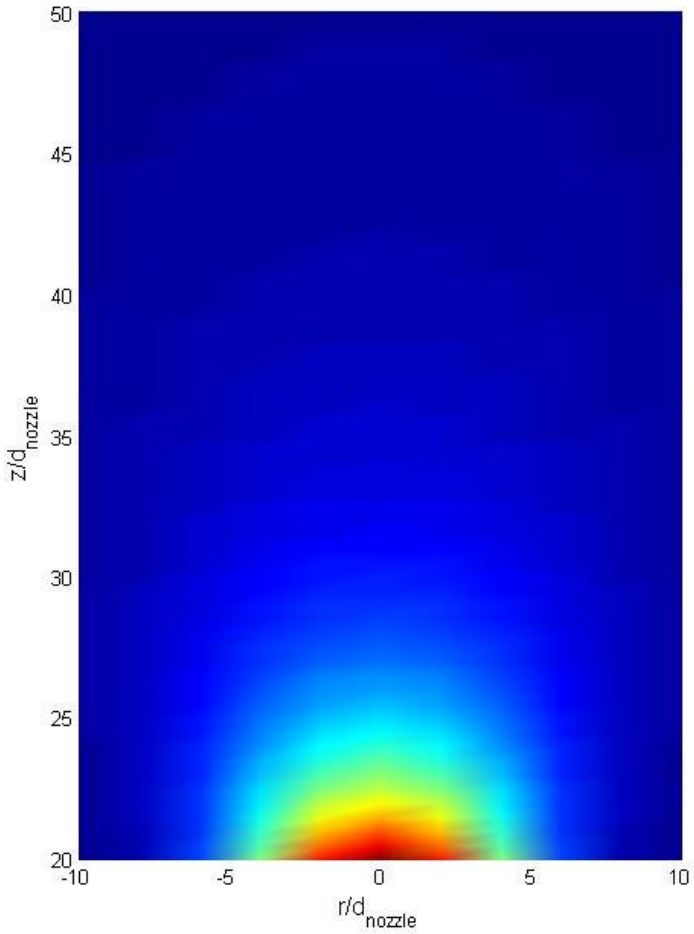

Figure 7: Energy dissipation rate of a turbulent round jet

Chapter 2: Experimental Methodology

2.1 Description of the Facility

The experiment was conducted within an octagonal acrylic tank, shown in Figure 8. The tank is approximately 1.8m tall and 1.2m across with a volume of 577 gallons. The size of the tank was designed to eliminate wall effects in the experimental area. The tank is filled and drained by four evenly spaced holes about the perimeter of its floor. Due to a tendency for filling to create a current within the tank, the water must be allowed time to settle before the commencement of experiments to insure that the water is quiescent. The top of the tank is equipped with a slot on each wall that empties into an overflow box. These boxes are attached to tubing that allows the excess fluid to drain. The boxes insure that when fluid is injected into the tank over the course of an experiment, the height of the waterline remains constant. This is especially important for longer experiments where enough water is injected by the jet to change the hydrostatic pressure of the experiment. The overflow boxes are also useful for experiments using buoyant oil. When the oil forms a film on the water surface, it is skimmed off by the overflow boxes thereby preventing droplet recirculation that could compromise the images being taken for the experiment. The tank also has an access door located on one of the side walls that can be used to clean the tank and make changes to the experimental apparatus.

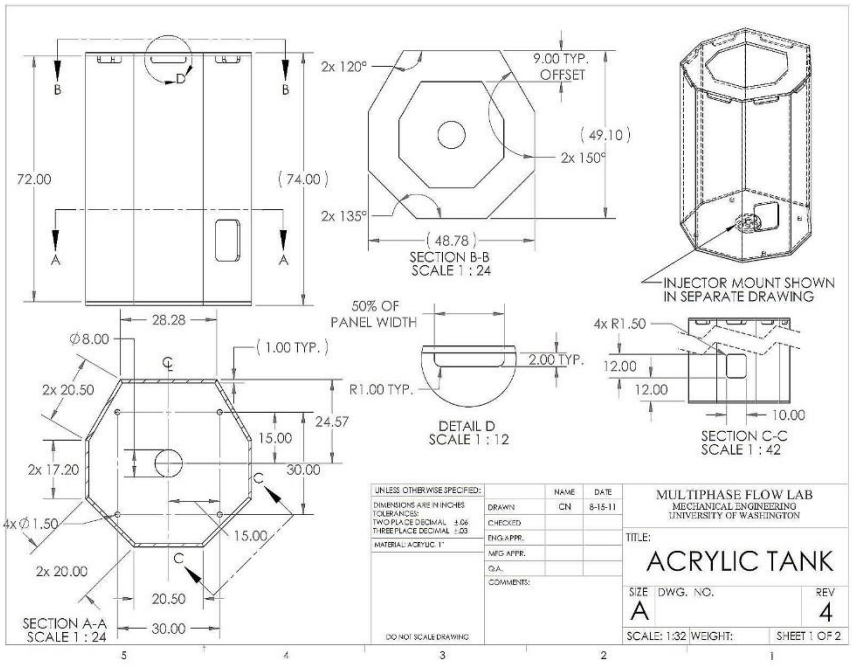

Figure 8: Drawing of octagonal acrylic tank

In the center of the tank floor there is a doughnut shaped piece of acrylic used to mount the jet nozzle. The interior profile of the nozzle follows the third order polynomial shown in equation 10 [11]:

$$r = \frac{d_i}{2} - \frac{3}{2}(d_i - d_j)\left(\frac{z}{L}\right)^2 + (d_i - d_j)\left(\frac{z}{L}\right)^3 \quad (10)$$

where *r* is the local radius, *z* is the vertical position, d_i is the initial diameter of the nozzle equal to 50mm, L is the length from the entrance to the exit if the nozzle equal to 42mm, and d_j is the exit diameter of the nozzle equal to 4mm. The nozzle can be seen pictured in Figure 9.

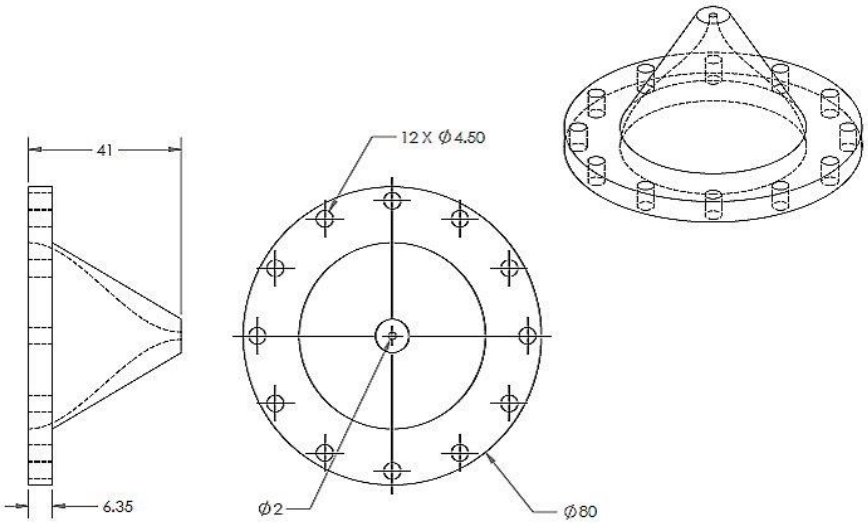

Figure 9: Drawing of nozzle

Water is injected through the jet nozzle from a pressurized bladder tank. The lower part of the tank is filled with water and the upper part of the tank, separated by a flexible diaphragm, is filled with air pressurized at 85 psi. The flow rate of the jet is controlled using a ball valve, and a needle valve, and measured with a turbine-type volumetric flow meter. The system is calibrated for up to 10 gpm with an accuracy of +/- 1%. The Reynolds number of the jet in the experiments was varied between 18,000 and 34,000 (0.9 and 1.7 gpm). The Reynolds number upper limit was determined by the amount of particle break-up occurring downstream of the injection location. Values of the Reynolds number were chosen above the critical value of 10,000, to allow for the highest turbulent intensity before breakup for each injection location.

2.2 Particle Injection System

The experiments performed for this study involved injecting a fluid, either air or canola oil, into a turbulent water jet. The fluid was injected using a dispensing needle bent at 90°, the needle used for the air bubbles was 27 gauge and the needle used for the oil droplets was 18 gauge. Different needles were required for each fluid in order to limit the head losses through the dispensing system and ensure that the bubbles and droplets were consistently of the smallest volume achievable. The dispensing needle was mounted on an adjustable stand, as pictured in Figure 10. The mount has a circular base, which allows it to be fixed relative to the center axis of the jet. The mount also allows for the fluid injection location to be adjusted radially and vertically with respect to the jet nozzle.

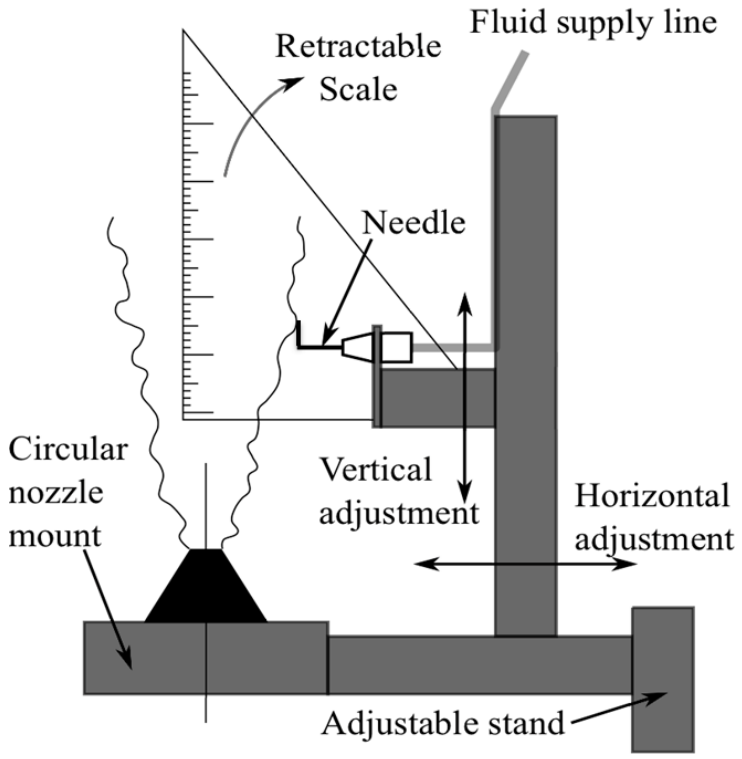

Figure 10: Schematic of needle mount

A syringe pump (NE-1000, New Era Pump Systems Inc. Somewhere, MA), was used to produce the injecting pressure to drive the particles into the jet. It is a linear displacement pump with an electronic flow rate control. when injecting air bubbles, a plastic, 38 mm diameter syringe was used, while oil

droplets where injected from a glass, 28 mm diameter syringe was used because the plastic syringe used for air had a much tighter seal to prevent leakage and depressurization. The glass syringe used for oil injection had much lower frictional losses so the pump was able to overcome the head losses associated with the higher viscosity fluid.

The particles were injected at five different injection locations. At a height of 20 jet diameters above the nozzle, particles were injected at 1, 1.5, and 2 half-widths from the centerline of the jet, and at 35 jet diameters from the nozzle particles were injected at 1 and 1.5 half-widths from the jet centerline. As explained in section 0, the radial half width is the location within the jet where the mean velocity is half of the centerline velocity, making it a function of vertical position. These locations can be seen in Figure 11 below.

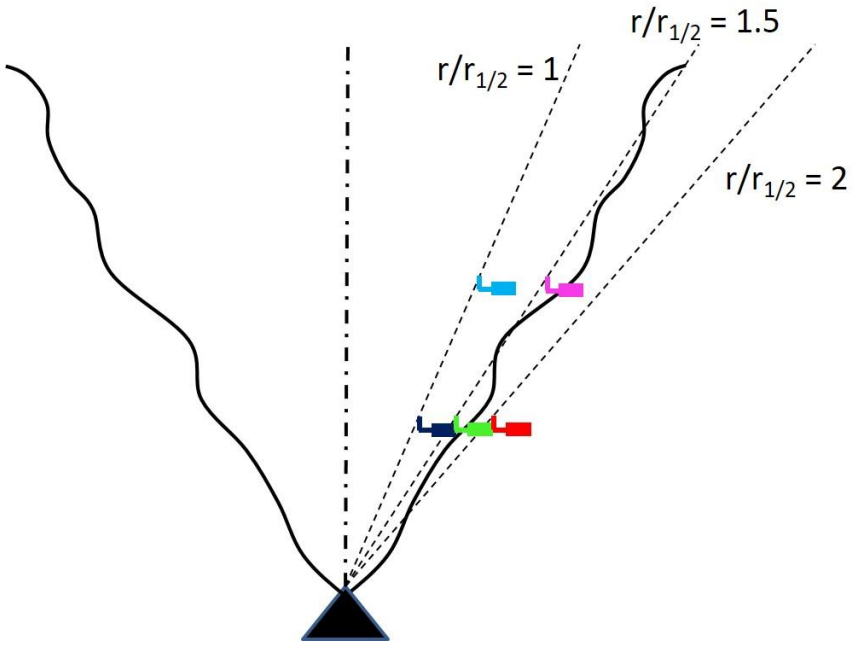

Figure 11: Particle injection locations

2.3 Properties of Injected Fluids

Air bubbles and canola oil droplets, whose properties can be seen in Table 1, were injected and tracked in this study to determine their dispersion. The air bubbles were injected into the jet at a rate of 1 ml/min. For oil droplets, the injection rate was set at 0.8 ml/min at the vertical distance of 20 diameters, while for the vertical distance of 35 diameters, the oil droplets injection rate was 1.2 ml/min.

The injection rate did not affect the size of injected particles, only the speed at which they were injected, therefore a rate was chosen that produced the highest number of particles that the post processing software was able to identify and track within the image.

Table 1: Injected fluid properties at 25C

	Air	Canola Oil
Density (kg/m^3)	1.18	913
Specific Gravity	0.0012	0.92
Surface Tension (N/m)	0.072	0.032
Dynamic Viscosity (Ns/m^2)	1.96e-5	5.70e-2

2.4 Particle Size Measurements and Control

The size of the particles injected into the jet is dependent on how the stream of fluid pinches off from the tip of the needle. When air is injected into the jet a spherical bubble forms immediately after leaving the needle. In contrast, when oil is injected into the jet it remains connected to the needle and deforms with the passing of turbulent eddies. The oil is eventually pinched off from the needle and continues to break up within the jet until the droplet is small enough that is no longer subject to bulk deformations. These methods of injection can be seen in Figure 12. In order to neglect the effects of particle deformation, particles were only recorded if they had a circularity $\left(4\pi \frac{\text{Area}}{\text{Perimeter}^2}\right)$ of 90% or higher. Although the mechanism for this droplet/bubble formation is beyond the scope of this investigation, it was observed that the size of the fluid particle is dependent on the turbulent energy dissipation rate at the location of injection. As can be seen in Figure 13, the injected particles (air bubbles or oil droplets) are approximately 1mm in diameter, with particle size depending in their injection location and decreasing logarithmically with turbulent energy dissipation rate.

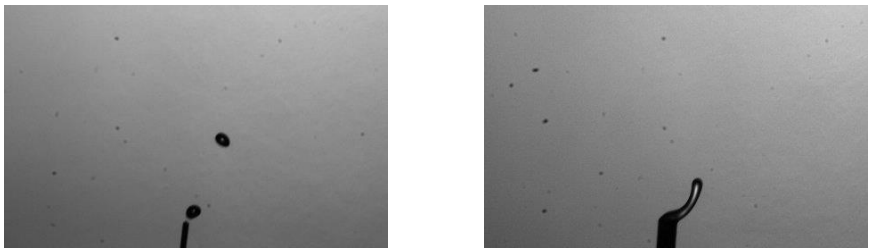

Figure 12: Injection of air (left) and oil (right)

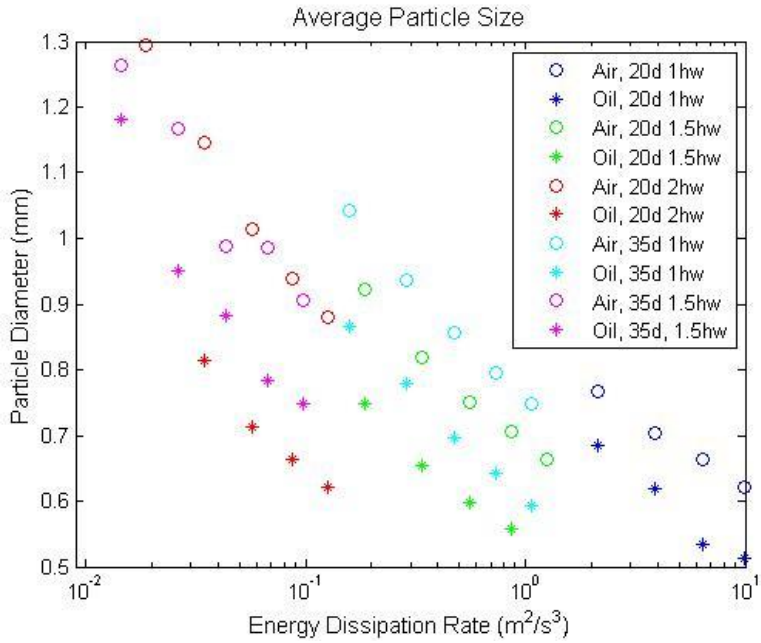

Figure 13: Particle sizes at various injection locations

2.5 High-Speed Imaging

High-speed imaging was employed to capture the movements of the fluid particles as a basis to reconstruct their trajectories. High-speed videos of the particles were taken using backlit shadowgraphy. A LED light (Constellation 120, IDT Vision Ltd, Pasadena, CA) was used to illuminate the particles in the field of view of the camera. This type of light was chosen for its high intensity output (20,000 lumen), necessary for very short exposure photography, and for its uniformity in both space (with an adequate spatial diffuser) and in time (with no trace of the 50 Hz electric grid frequency typical of incandescent lamps).

A 1 MPixel, CMOS high-speed camera (Phantom V12, Vision Research Inc, Wayne, NJ) was used to capture the images. The camera was placed coaxially with the lamp, as shown in Figure 14, so that the collimated light would be captured by the camera, and rays scattered by the bubbles or droplets would not reach the camera sensor, making it simple to determine the silhouette of the particles from the shadows created by light reflection and refraction on the particle surfaces and media. This technique generates a large contrast between the particle outlines and the background making it easier to identify the area-projection of the particles onto the image sensor during post processing of the images. The field of view was adjusted to 8 cm by 5 cm, with the long axis oriented vertically along the mean flow direction, using a Macro 180 mm lens (Tamron Inc. Japan), resulting in a spatial resolution of 65 microns per pixel (or a magnification of M=1/3).

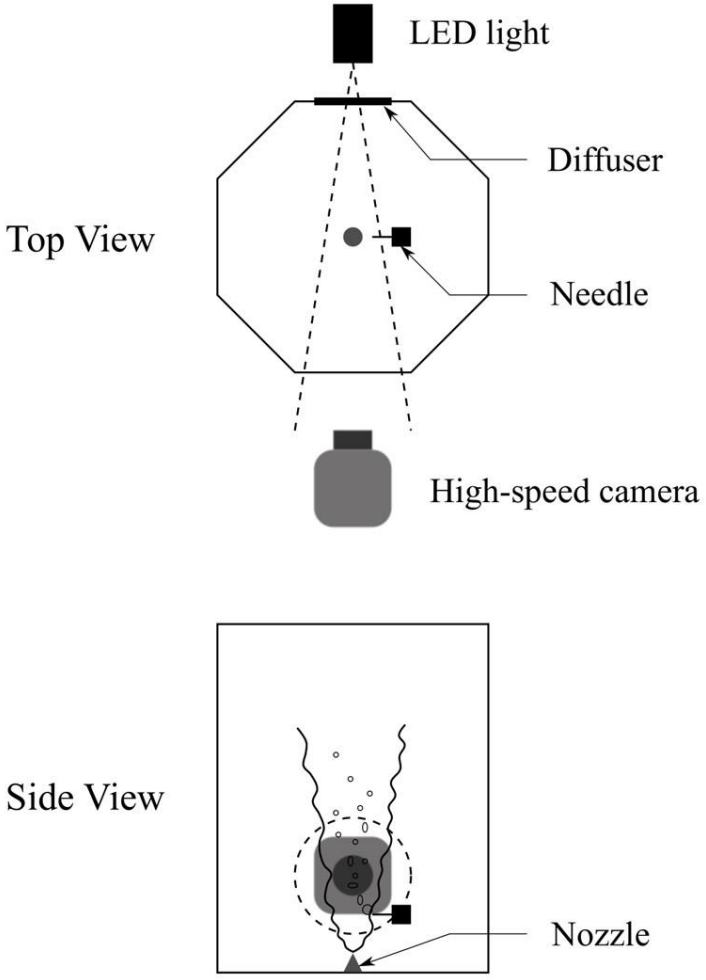

Figure 14: High speed imaging set-up

Chapter 3: Particle Tracking

3.1 Particle Identification

Once the images have been taken, they must be analyzed to determine the locations, sizes, and shapes of the particles. The software used was ImageJ, an image processing software developed by the National Institutes of Health. Before each test, an image was taken of the background with the same settings as the test. The background was then subtracted from the test images to remove the effects of non-uniform back lighting. Once the background is subtracted, the images are sharpened and then thresholded. Thresholding converts a grayscale image to a black and white, binary image. Any grayscale value above there threshold value is converted to white and any below to black. Once the image has been converted to black and white, ImageJ analyzes the particles using a built-in function. This function records the size, position, and circularity of the particles in every image. An example of a processed image and the data extracted from it is shown in Figure 15.

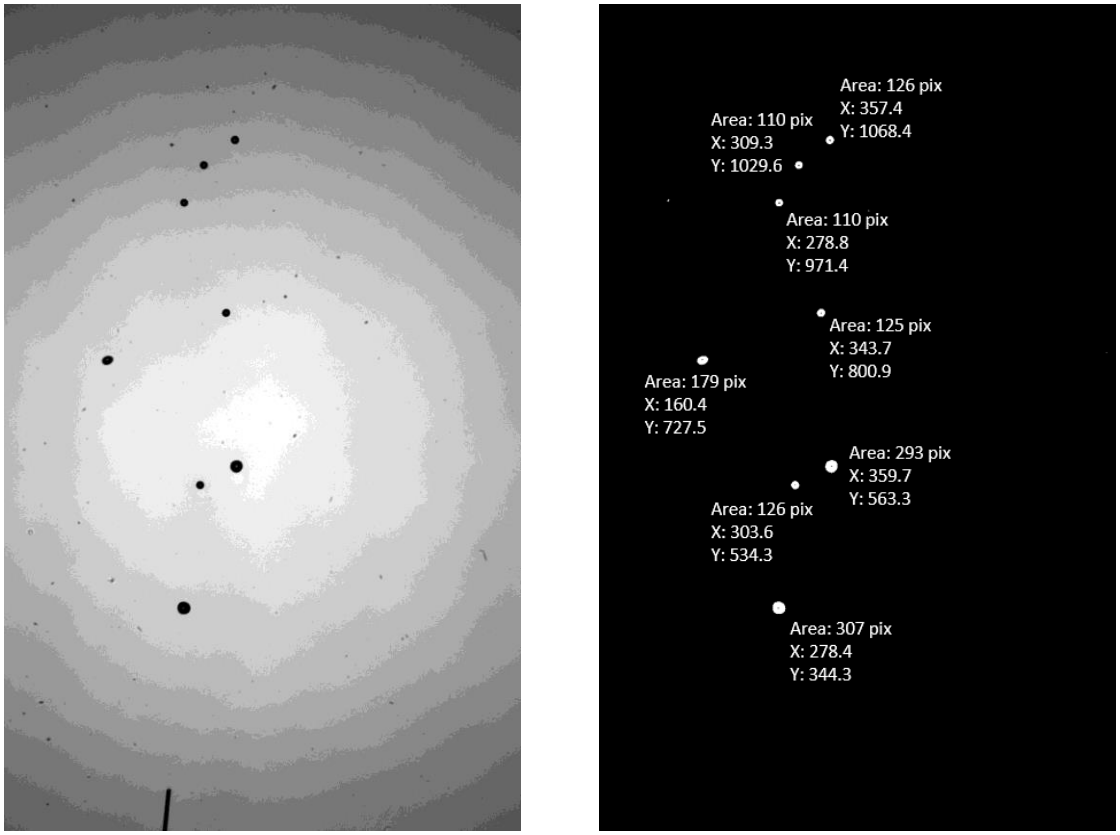

Figure 15: Image of air bubbles before and after processing

3.2 Particle Tracking

Once the images have been analyzed and the particle data recorded, the path of each particle must be determined. Typical particle tracking methods find a track, then find the best particle to continue the track. For this experimental set-up, the high local density of particles and the large velocity fluctuations result in close to 50% error for this method. The problem occurs because if a particle is the best match for two different tracks, it will be assigned to both of them and the particle that should have been assigned to the second track will be assumed to be the start of a new track. Then for the next image, the particle will again be assigned to both tracks resulting in double counting of one track and an incorrect start of the other. The tracking method has therefore been modified so that each particle can only be assigned to one track. This decreases the tracking error by eliminating the double counting of particles.

Tracking used a combination of a three and four frame approach. The three frame approach starts with the position of the particles when they first appear in the field of view in image *n* (Figure 16a). This initial position is the first entry in the track. The program then attempts to match each particle in image *n+1* with an existing one-entry track. The matching is done by finding the triplet that minimizes the acceleration (**a**) between each track from image n, the particle in image *n+1*, and each particle in image *n+2* where $\mathbf{a} = \mathbf{x}_{n+2} - 2\mathbf{x}_{n+1} + \mathbf{x}_n$. Using this method, if there are *b* existing tracks and *c* particles in image *n+2*, there will be *a*b* possible accelerations for each particle in image *n+1* (Figure 16b). The particle in *n+1* is then assigned the track that allows for the smallest acceleration (Figure 16c).

Once a track is two images long, the method advances to a four frame approach (Figure 16d). This method matches each particle in image *n+2* to a track established from images *n* and *n+1*. For each particle in image *n+2* and each existing track (containing a pair of particles from images *n* and *n+1*), the expected position of the particle in *n+3* is estimated with the equation $\boldsymbol{x}_{\boldsymbol{n+3}}^{\boldsymbol{expt}} = \boldsymbol{x}_n - 7\boldsymbol{x}_{n+1} + 5\boldsymbol{x}_{n+2}$ Then, each particle in image *n+3* is examined and the distance between the actual and expected position of the particle is compared. For each particle in image *n+2*, the track is chosen that minimizes the distance between the estimated and actual position of the particle in image *n+3* as long as this particle exists within a specified search area around the expected position of the particle in image *n+3*. However, if there are no particles within a specified search area for any of the tracks, the particle in image *n+2* starts a new track. This process continues for all the images, using the three frame approach if the existing track is only one image long, and using the four frame approach if the track is two or more images long.

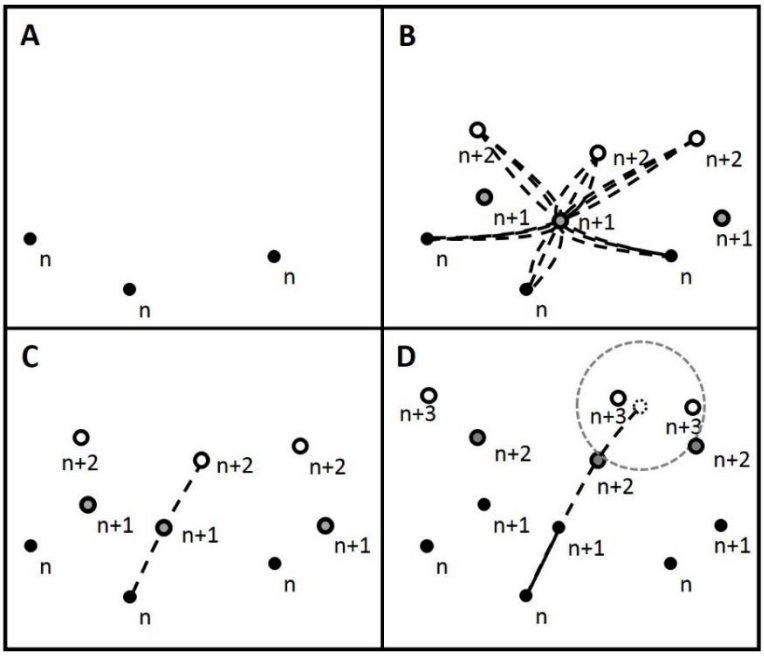

Figure 16: Particle tracking illustration

3.3 Tracking Corrections

Once the initial tracking is completed, the tracks are corrected for common errors. The first of these errors is an incorrect assignment of the first data point in a track. This error occurs because only one track can be assigned to each particle and priority is given to the particle listed first. Therefore, if the initial position of a track is within the tolerance of an existing track, it will be assigned to that track and the correct particle will be forced to start a new track. This results in two data points for the image being switched. This error is corrected by taking into account the cross-sectional area of the particle, as well as its position to determine if the first data point in a track is incorrect. To correct this error, the first data point in each track is examined and compared to the other tracks at the same time. If, at a given time, there are two particles (A and B) within the frame of view there will be two tracks (A and B) associated with that time. If the first data point in track A is point A, the area, x-position, and y-position of point A will be compared to the average of the next three points in that track. Similarly, point B is in track B at the same time step as point A. Point B is compared to the average of the four points surrounding point B. If the difference between point B and the average of the points in track B is larger than the difference between point B and the average of the points in track A for all three

measurements, and correspondingly for point A, then points A and B will be switched. If all the indicators do not match, the original tracking will stand.

Another common error in the particle tracking algorithm is that it ignores crossing particles. Because the particle images are taken in two dimensions and the actual particle movement occurs in three dimensions, particles can appear to occupy the same position in the images. When this happens, the particle identification algorithm perceives only one particle for the time that the two particles overlap. This type of event is identified by the tracking correction algorithm from the positions of the two particles directly before and after the overlap occurs. Crossing particles are searched for based on the knowledge that all particles have their initial position close to the location of the dispensing needle. Therefore, when the initial position of a particle is not near the tip of the dispensing needle, it is likely the result of two particles moving apart after overlapping. When this occurs, the tracks are examined to determine if there is another particle in a very similar location at the same time. If so, the algorithm attempts to match the position of that track with a track that ended a few frames before, signifying the time step when the particles initially overlapped. Once these two times are identified, the areas of the particles are compared before and after overlapping to make sure the particles do not switch tracks after overlapping.

The last common error that the algorithm corrects for is when tracks end unexpectedly. Because the particles are generally moving vertically through the field of view, most tracks terminate at the upper edge of the image. If this does not happen, either the particle moved out of the horizontal view of the camera, or the track was terminated prematurely. Tracks often terminate prematurely when the particle moves out of the search area of the tracking algorithm. In order to correct this error, the algorithm attempts to match the unexpected end of one track with the unexpected beginning of another. A track could also end unexpectedly if the particle identification algorithm fails to identify the particle because of its size or index of refraction. In this case the algorithm attempts to match the unexpected end of one track with the unexpected beginning of another but at a later time, the location of the intermediate points are interpolated linearly.

Chapter 4: Experimental Results

The behavior of the particles after they are injected into the flow depends on the particles' buoyant force, the location of the particles within the jet, and the Reynolds number of the jet. In order to vary these parameters systematically, tests were conducted using both air bubbles and oil droplets, at five different particle injection locations, and with five different jet Reynolds numbers. The experimental data was obtained using the techniques described in chapter 2. Approximately 10,800 images were taken for each experimental condition, which is equivalent to approximately 18 seconds of testing. The analysis in this chapter is based on those 50 different experimental conditions, which can be summarized with four non-dimensional numbers: Jet Reynolds number, density ratio, and non-dimensional radial and axial positions. Alternatively, these represent four physical non-dimensional numbers: the density ratio, the non-dimensional shear rate, the turbulence Reynolds number and the turbulence intensity (these last three at the location of injection).

4.1 Particle Vertical Velocity

When the particles are injected into the flow, they are approximately stationary as they come out of the needle. They then accelerate due to the interactions with the fluid, until they adjust to the fluid velocity plus a terminal velocity due to buoyancy. This can be seen in Figure 17. The air bubbles reach their terminal velocity more quickly than the oil droplets because their higher buoyancy and lower inertia allows them a faster response to equilibrium. Once the equilibrium state has been reached, the velocity of the two types of particles is similar, with air bubbles being only slightly faster in the vertical direction than oil droplets. The locations of the particles were recorded in two dimensions, with a small uncertainty in the radial position of the particles given by the depth of field of the camera, therefore the mean velocity of the flow at each particle location cannot be fully determined. All particle velocities are compared to the centerline velocity at the given vertical location, as an upper bound of the ambient fluid velocity that accelerates the particles along their trajectories. The particle velocities rise from their injection values but always stay below the centerline velocity, even as it decreases with distance from the jet, since these are low inertia particles, there is physical possibility of the particles average velocity overshooting the centerline velocity of the jet.

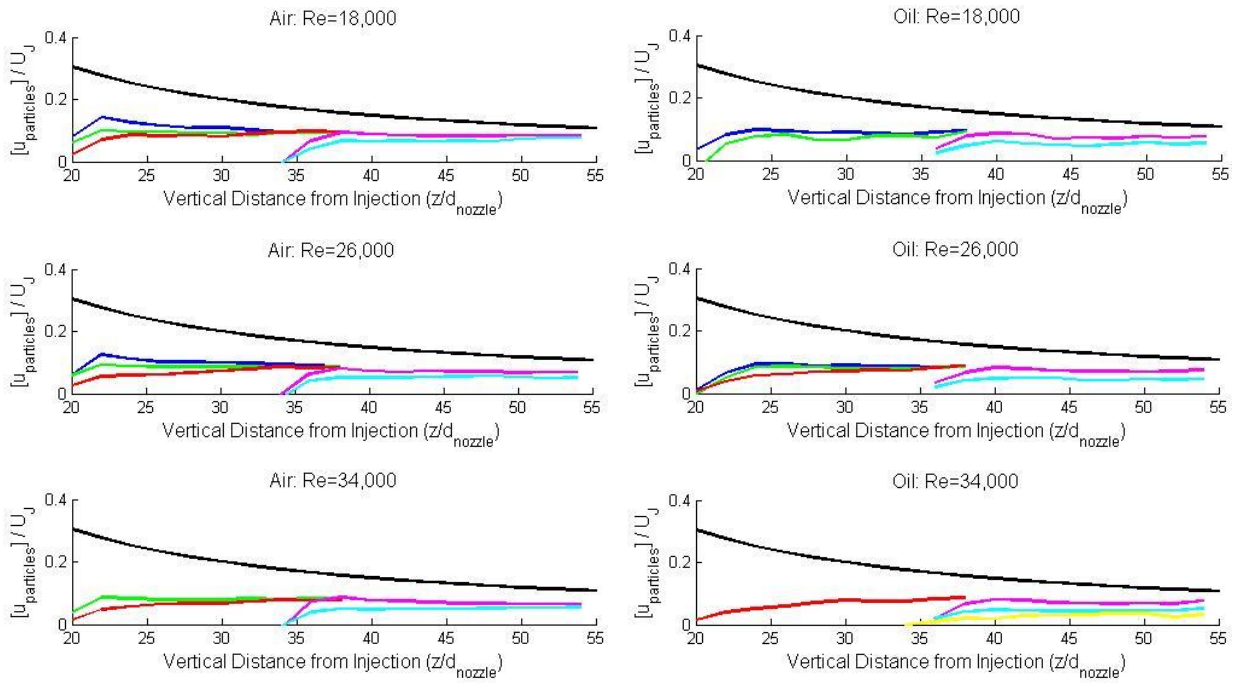

Figure 17: Vertical velocities of air bubbles and oil droplets. Black lines represent the centerline jet velocity (made non-dimensional with the jet velocity at the nozzle), as an upper bound of the velocity at that axial plane (z/d = constant).

Another measurement of interest is the turbulent fluctuations in the particle motion, which can be seen in Figure 18. This is calculated by dividing the root mean square of the particle velocity by the mean particle velocity. The turbulence fluctuations are high at the point of injection (where fluctuations are strong and the mean particle velocity is close to zero) and then quickly decrease as the particles accommodate to the ambient fluid velocity and their own terminal velocity.

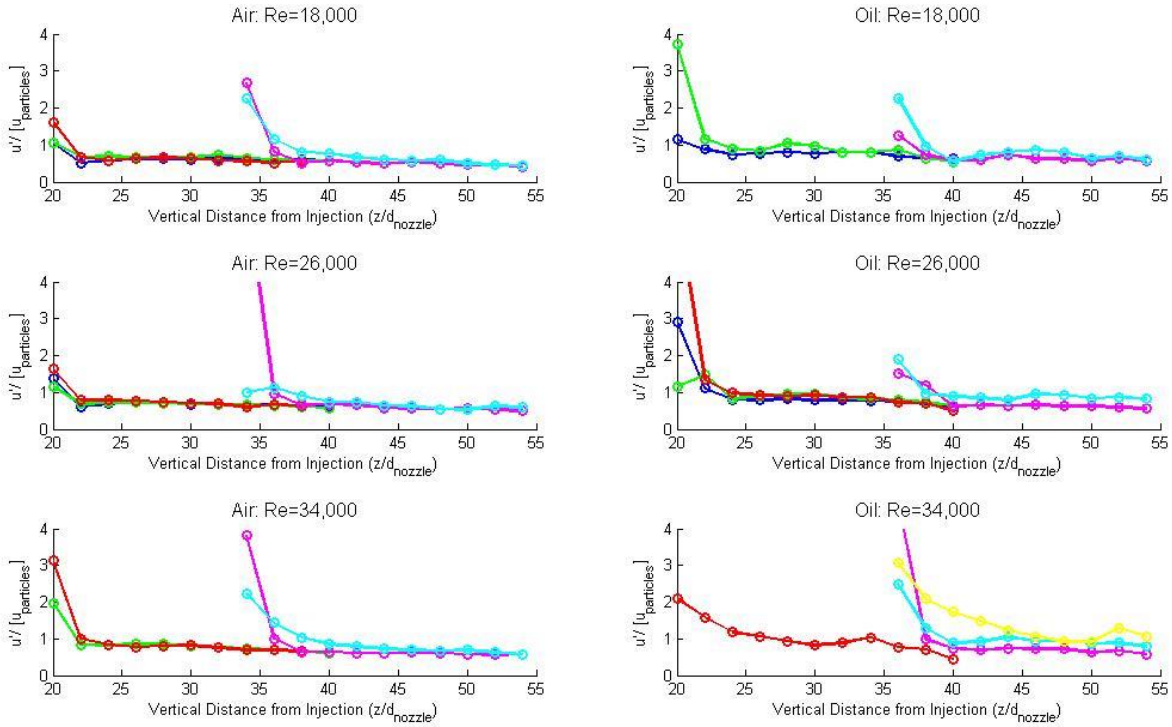

Figure 18: Turbulent fluctuating vertical velocities of air bubbles and oil droplets, made non-dimensional with the particles' mean velocity

4.2 Particle Acceleration

Because the particles are initially quasi-stagnant when injected into the jet, they quickly accelerate to the flow velocity, due to the strong drag and the low inertia. As seen in Figure 19 and Figure 20, this results in very large accelerations immediately following injection. These accelerations increase with Reynolds number and injection position because they depend on the local jet velocity, and the higher Reynolds numbers and closer injections to the nozzle result in faster jet flow velocities. After their initial vertical acceleration, the particles experience an overshoot which results in a short transition into negative accelerations, shown in Figure 20. This dip is especially noticeable with air bubbles. The particles then experience a prolonged period of small, negative accelerations. This period corresponds with the approximately constant velocity discussed in the previous section. The accelerations are negative because the mean flow velocity decreases with distance from the nozzle so the velocity of the particles is also decreasing.

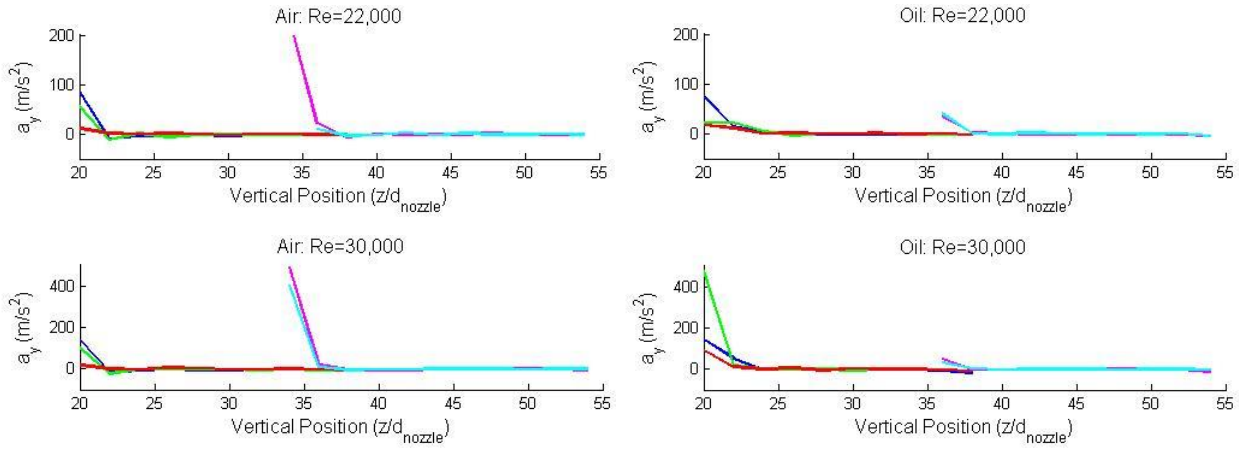

Figure 19: Initial particle accelerations

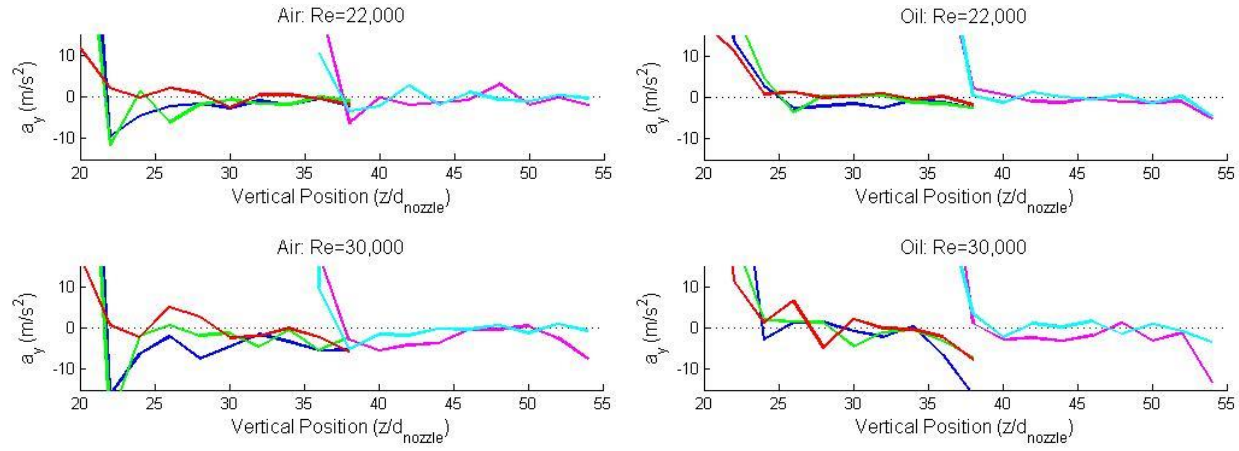

Figure 20: Long-term particle accelerations

In addition to the vertical accelerations, due primarily to the mean flow, it is of interest to compute the accelerations in the horizontal direction, due primarily to interaction with the turbulent eddies. The direction of the acceleration is not physically significant, so the absolute value of the horizontal particle acceleration is shown, in Figure 21. In parallel to the observations in the vertical acceleration discussion, the horizontal acceleration is large when the bubbles are first injected and then decreases as the particles continue within the jet. The particles are injected with zero velocity and so accelerate to reach the local flow velocity, including large scale eddies, in the first instances. As they reach the fluid instantaneous velocity, the accelerations are reduced to values consistent with that induced by the turbulent eddies on a fluid particle. The particles injected at 20 diameters above the nozzle and two

half-widths from the centerline (shown in red) have a significantly smaller acceleration in the horizontal direction than those at other injection locations. This is because this location is much farther from the center of the jet than the others, in terms of mean velocity and turbulence intensity, so the strength and frequency of the turbulent eddies acting on the particles is significantly reduced, compared to the other injection locations, and thus the acceleration induced on the particles is much lower.

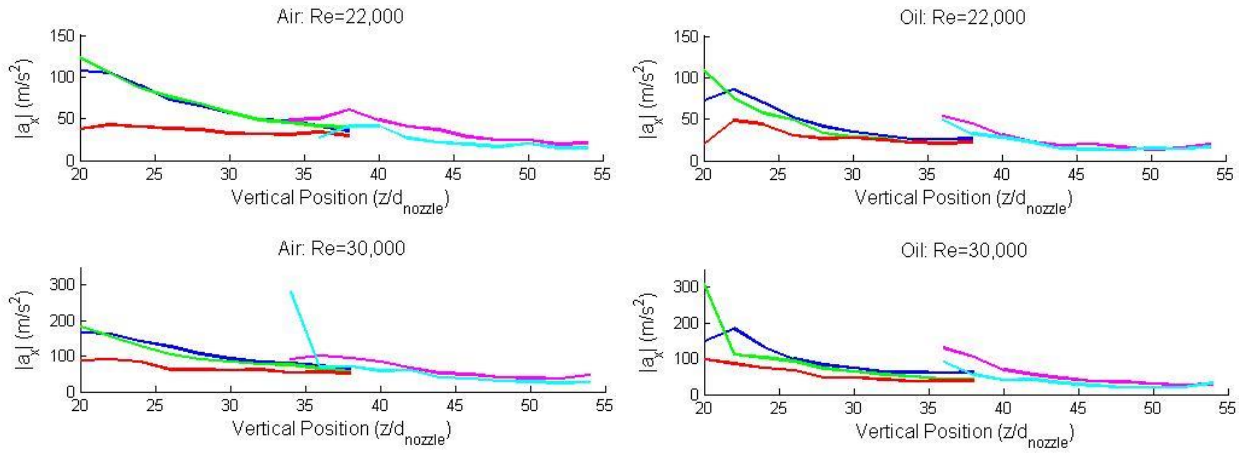

Figure 21: Horizontal particle accelerations

4.3 Single Particle Dispersion

Once the paths of the particles had been tracked, their displacements from their initial position could be measured as a function of time. The mean square of these displacements, the dispersion of particles from their source, can be seen in Figure 22. The mean square displacement of air bubbles and oil droplets, for various jet Reynolds numbers, are shown for one particular injection location (z/d=20 and $r/r_{½}$=1). Air bubbles disperse much more quickly than the oil droplets, most likely due to their larger buoyancy and terminal velocity. The buoyant force does not have as large of an effect on the oil droplets because their density is much closer to that of water.

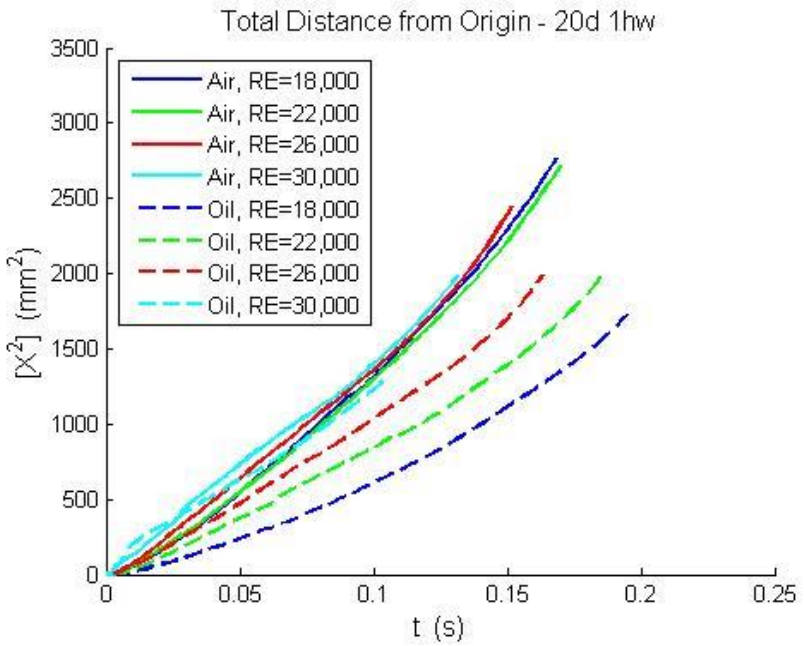

Figure 22: Single particle dispersion, injected at 20 diameters, 1half-width

Additionally, the Reynolds number of the jet has a much larger effect on the oil droplets than the air bubbles. While the air bubbles disperse at approximately the same rate for all Reynolds numbers when injected at the same location, the oil droplets disperse much more quickly in higher Reynolds numbers. As discussed in section 0, the size of the particles injected is affected by the turbulent dissipation rate at the injection location. Therefore, the size of the oil droplets injected at a given location decreases as the jet Reynolds number increases. This change in particle size is investigated as the potential reason for the differences in dispersion for different Reynolds numbers. Figure 23 shows the size distribution of particles injected 20 diameter downstream of the nozzle and 1 half-width from the centerline. As expected from section 0, the oil droplets are smaller than the air bubbles, and there are some slight differences in size distribution for different Reynolds numbers. To correct for this difference, the data is filtered so that only air bubbles with a diameter between 0.65 and 0.75mm and oil droplets with a diameter between 0.35 and 0.45mm are considered. The single particle dispersion for this narrow size class can be seen in Figure 24.

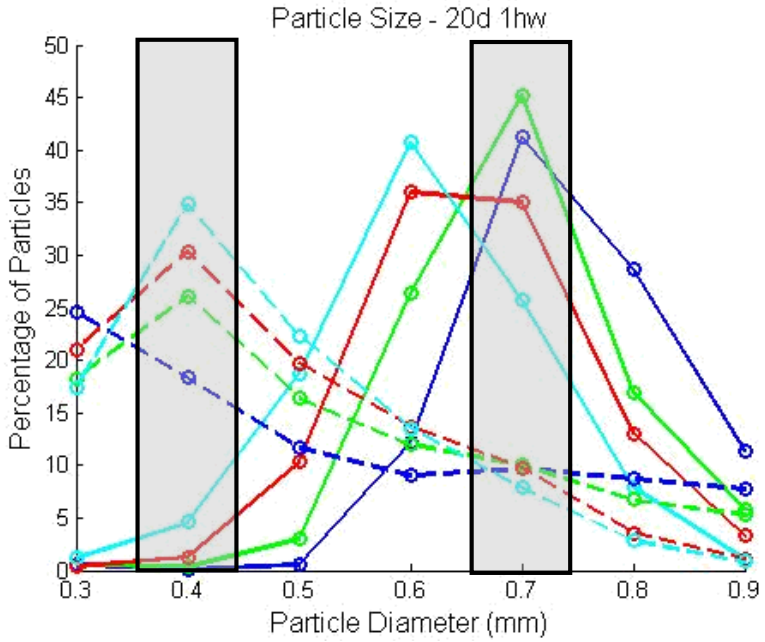

Figure 23: Size distribution of air bubbles (solid lines) and oil droplets (dashed lines) injected for different Reynolds numbers.

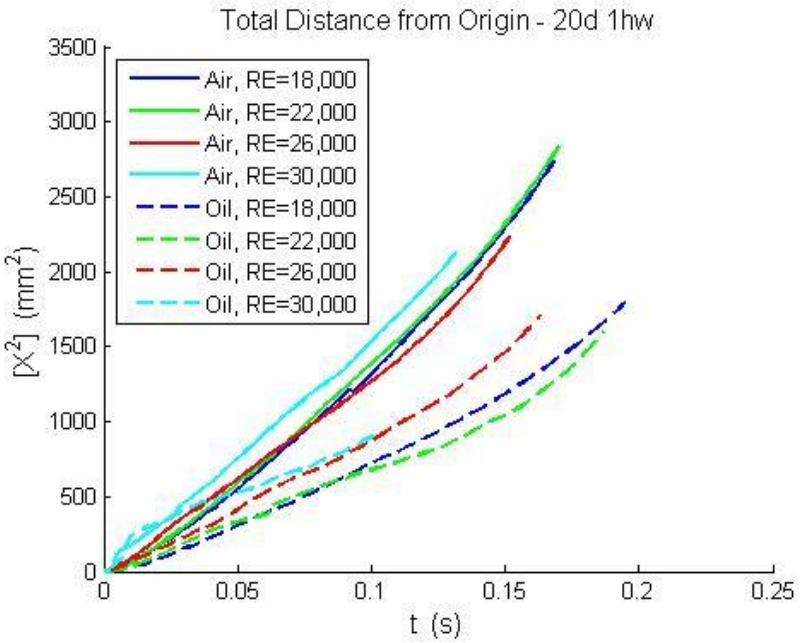

Figure 24: Single particle dispersion of particles with constant size, injected at 20 diameters, 1half-width

When particles in the narrow size range are considered, the relationship between single particle dispersion and Reynolds number becomes weaker for oil droplets. However, the dispersion of air bubbles does not change. The apparent correlation between single particle dispersion and Reynolds number observed in Figure 22 was primarily due to the variation in particle size which affects both the particles' inertia and terminal velocity. This comparison between air bubbles and oil droplets shows that, for the conditions in these experiments, the rate of dispersion is influenced by the particle's buoyancy. The Reynolds number of the jet is high enough in all experimental cases that no strong effects are observed.

A similar analysis was conducted to examine the effects of the particle injection location on single particle dispersion. This is shown in Figure 25 for particles within a constant size range. In general, air bubbles disperse more quickly than the oil droplets, but this is not always true. For injection locations 20 diameters and 1.5 half widths, and 35 diameters and one half width, oil droplets disperse at a rate similar to air bubbles. Additionally, although in general changing the injection location has a smaller effect on the air bubbles than the oil droplets the variation between locations for air bubbles is much greater than that between Reynolds numbers.

From these first set of observations, we can conclude that air bubbles disperse more quickly that oil droplets due to their larger terminal velocity, and that injection location (shear rate and turbulence dissipation rate) has a larger effect on dispersion than the jet Reynolds number, for this large Reynolds number above the critical mixing transition.

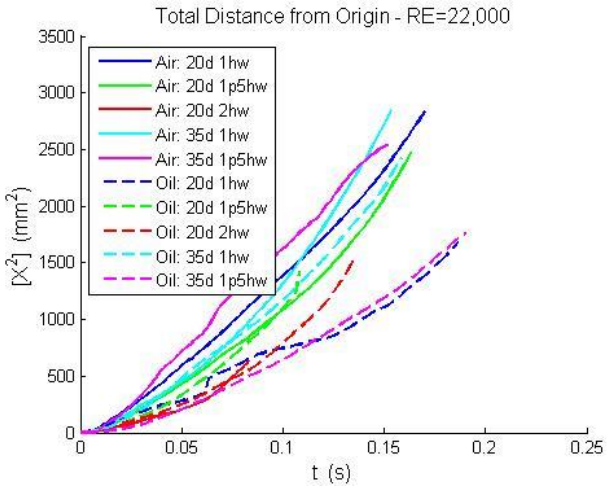

Figure 25: Single particle dispersion injected at RE = 22,000

Given the effect of the buoyancy of the particles on their displacement from the injection location, the total mean square displacement does not provide a good measure of the effect of turbulence on dispersion. Therefore, the horizontal displacement is examined. By focusing on the horizontal dispersion, the effect of the particles' terminal velocity will be limited to how the particles interact with the turbulent eddies.

As seen in Figure 26, the horizontal dispersion of particles increases with Reynolds number. For all Reynolds numbers tested, the air bubbles disperse more quickly than the oil droplets. The particles initially disperse rapidly and then level off to approximately a constant distance from their injection location, as they are flung out of the jet into a stagnant region. This tendency is more pronounced for higher Reynolds numbers. Similar trends were observed in Figure 27, which compares horizontal dispersion at different injection locations. The dispersion increases with increasing turbulence dissipation rate. These trends, however, are not as clear as for the various Reynolds numbers. Scaling arguments and comparison with Taylor's dispersion in homogeneous isotropic turbulence are given in the chapter 5.

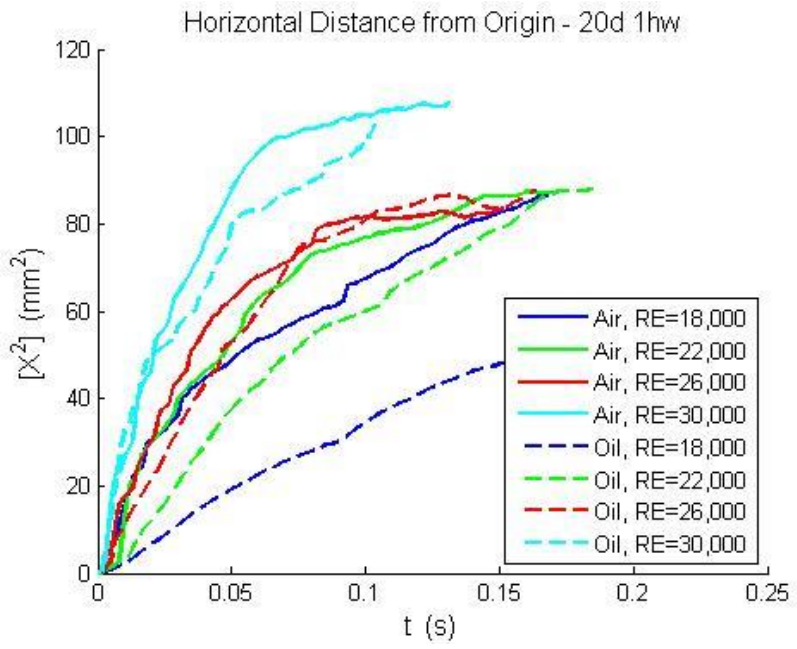

Figure 26: Single particle horizontal dispersion, injected at 20 diameters, 1half-width

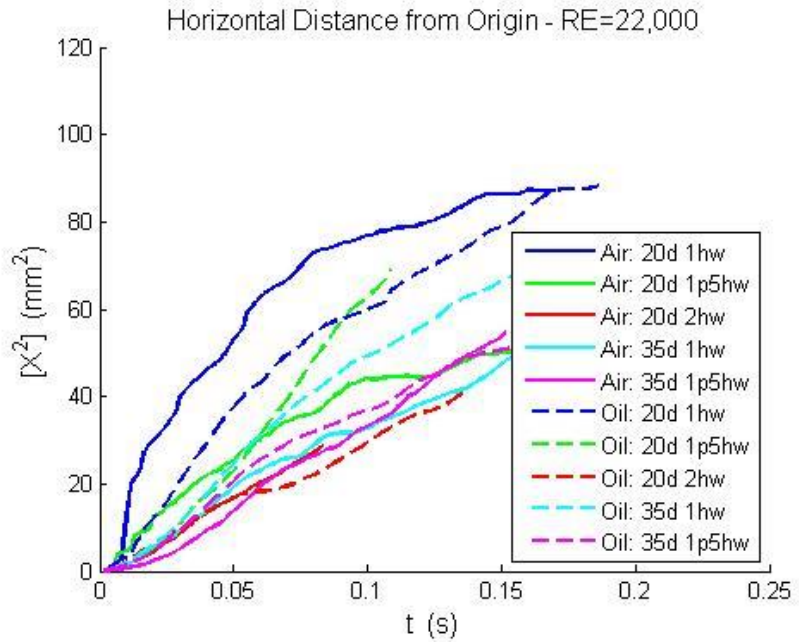

Figure 27: Single particle horizontal dispersion injected at RE = 22,000

4.4 Pair Dispersion

Pair dispersion examines the relative separation of two particles as they move through the jet. For this analysis, particles were paired if they had an initial separation of less than one jet diameter (4mm) and a difference in cross sectional area of less than 20%. The initial separation of the particles was controlled to insure that the particles were subjected to turbulent fluid velocities that were correlated. The cross sectional area was controlled to insure that the particles had similar terminal velocities. The separations of the pairs were then averaged over a set of 50 particles to determine the rate of dispersion at each injection location and Reynolds number.

First, the pair dispersion of particles injected at the same location is examined, one of these tests can be seen in Figure 28. The dispersion is quadratic with time. Unlike with single particle dispersion, the oil droplets tend to disperse faster than the air bubbles for the same Reynolds number and injection location. The relative separation of the particles is less affected by buoyancy than single particle dispersion. The common influence on buoyancy on particle trajectories, for the same density and diameter of the particles, will not affect the separation. However, buoyancy is still important in pair dispersion due to its effect on the particles interactions with the turbulent eddies, via the crossing

trajectories effect discussed in section 1.2. Figure 28 also shows that the rate of dispersion depends weakly on the jet Reynolds number, with slightly faster dispersion for higher Reynolds numbers.

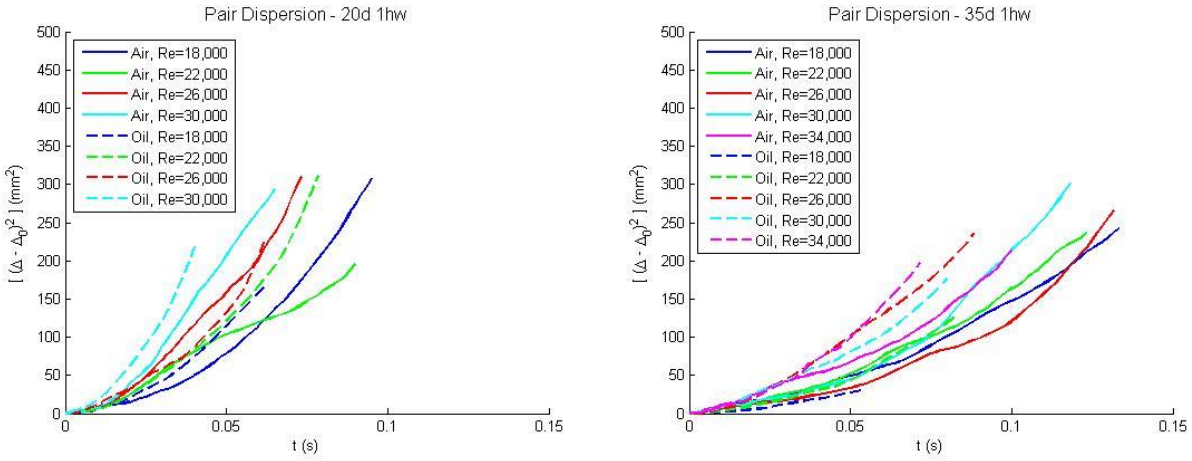

Figure 28: Pair dispersion injected at a constant location

The most determining factors in the pair dispersion is the shear rate and turbulent dissipation rate associated with injection location. A quadratic curve was fitted to the dispersion for all cases at each of the injection locations, in an effort to find the trends of particle pair dispersion. These curves can be seen in Figure 29. The rate of dispersion decreases with vertical distance from the nozzle, as both the shear rate and the turbulent dissipation rate decrease. Additionally, the dispersion increases with distance from the centerline. This is difficult to interpret because both the shear rate and the turbulent dissipation rate decrease for radial positions beyond the half-width of the jet. However, the turbulent dissipation rate decreases much more slowly than the shear rate so the increase in dispersion may be because the dispersion at small radii is dominated by shear and at large radii it is dominated by the turbulent eddies.

Mathematically, within the region of interest, the linear term has much more of an effect on the dispersion for particles injected at one half width than for particles injected at larger radii. The ratio between the linear and quadratic terms for the different injection locations can be seen in Table 2.

Figure 30 shows the pair dispersion for different injection locations at a two different constant Reynolds numbers. Large discrepancies are found between the different conditions, with no identifiable trends.

Dispersion for different injections locations at a fixed Reynolds number presents inconsistent results, with some cases showing higher dispersion for air versus oil and vice versa, and others showing higher dispersion for injection locations closer to the centerline, while some cases are higher for positions further from the centerline. The only consistent result is that injection locations further downstream from the nozzle lead to slower dispersion, as would be expected from lower shear and dissipation rates. It is apparent from these results, that injection location is more determinant of pair dispersion, through turbulent dissipation rate and mean shear rate, than the jet Reynolds number.

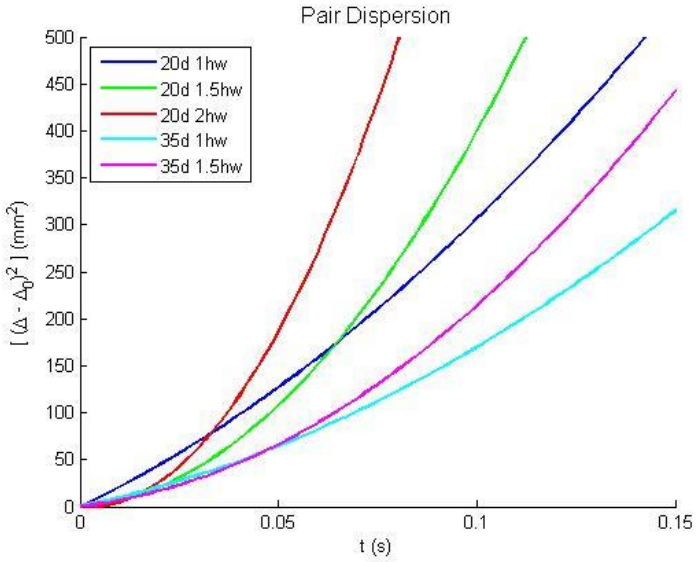

Figure 29: Quadratic curve fits for various locations

Table 2: Ratio of linear and quadratic coefficients

Injection Location	Linear coefficient/ quadratic coefficient
20d, 1hw	0.19
20d, 1.5hw	0.008
20d, 2hw	0.004
35d, 1hw	0.11
35d, 1.5hw	0.03

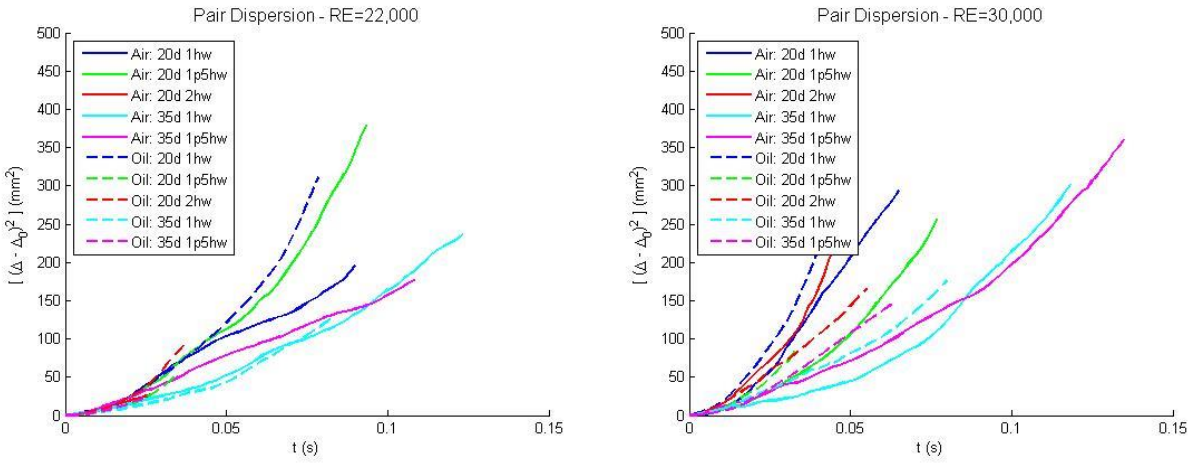

Figure 30: Pair dispersion injected at a constant Reynolds number

Chapter 5: Analysis and Conclusions

5.1 Single Particle Dispersion

The analysis of single particle dispersion will be limited to the case of horizontal dispersion, as discussed in section 4.3 because it provides the closest comparison to the dispersion in homogeneous, isotropic flow discussed section 1.1. It was predicted by Taylor that the mean square of the distance a particle travels from its initial position scales quadratically with time for very small times, and then scales linearly with time. In addition to these two temporal regions, observations from the data suggest that within the turbulent jet there is a third region that scales with the square root of time. These three regions can be seen in Figure 31.

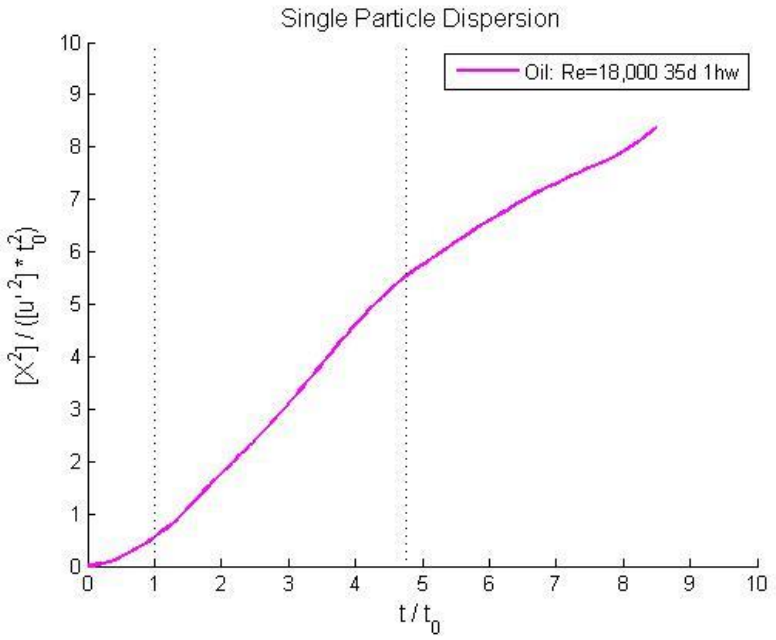

Figure 31: Single particle dispersion temporal regions

In the first region, the mean square of the dispersion scales quadratically with time. According to Taylor, the dispersion in the quadratic region is a function of the mean square of the fluctuating velocity. An example of this approximation can be seen in Figure 32. The figure shows that Taylor's quadratic equation is a good estimate for the dispersion, up to approximately the characteristic time: $t_0 =$

$\left(\frac{d_{part}^2}{\varepsilon}\right)^{1/3}$. The dispersion data were fitted to a quadratic function according to Taylor's theory, for times up to the characteristic time for each experimental condition. The ratios of the coefficients from the quadratic fit from the experiments to those from Taylor's theoretical prediction are computed for each injection location, as shown in Table 3. The measured values for oil droplets are closer to unity, more aligned with Taylor's theory, than for air bubbles. Oil droplets are smaller and with density ratio closer to unity than the air bubbles, thus, their behavior is more representative of fluid tracers, for which Taylor's theory was developed. Although dispersion was found not to vary widely for the different Reynolds numbers in the experiments, the results depended strongly on the injection location. The significant differences between Taylor's theory and the measured values of dispersion, and their widely differing ratios at the various injections locations, is hypothesized to be caused by the shear rate in the jet. The experiments subjected the particles to different rates of shear depending on the location they were injected in the flow, in contrast to the homogeneous isotropic turbulence conditions that are the basis for the theory developed by Taylor. Further analysis is needed to introduce the effect of shear on the particle dispersion into the theoretical model.

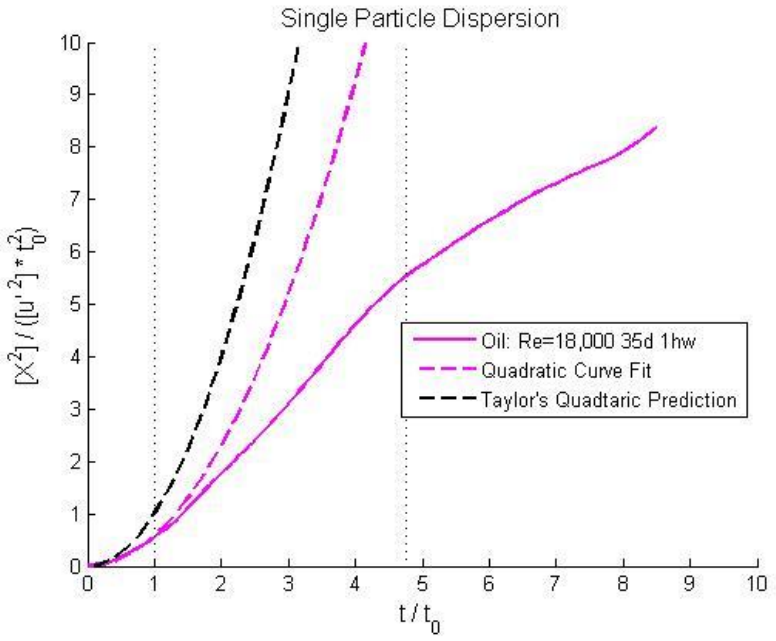

Figure 32: Quadratic fit for single particle dispersion as a function of time. Comparison of experimental data with Taylor's theoretical model.

Table 3: Ratio of experimental to theoretical quadratic fit coefficient

	Air	Oil
20d, 1hw	3.13	1.77
20d, 1.5hw	1.12	0.55
20d, 2hw	0.31	0.81
35d, 1hw	1.66	0.73
35d, 1.5hw	0.64	0.10

In the second region, the mean square of the dispersion scales linearly with time. According to Taylor, the dispersion in the linear region is a function of the mean square of the fluctuating velocity and the integral time scale of the turbulent fluctuations, calculated along the particle trajectories (Lagrangian). An example of the linear fit to the data can be seen in Figure 33. The figure shows that the slope of the experimental mean square dispersion is similar to the theoretically-predicted trend, for values of time after the characteristic time for the initial eddy turn over time. The experimental data is fitted to a linear function of time, in the linear region for each condition. The slopes of the fitted curves are compared to the theoretical values in Table 4. The comparison of the predicted and measured slopes are was again slightly better for oil than air and the ratios did not to differ greatly for different Reynolds numbers. The measured values were found to be closest to the predictions for injection locations that are farthest away from the jet nozzle. This result was unexpected because the flow far from the nozzle is more influenced by shear flow than the flow close to the nozzle, which is not taken into account in Taylor's equation. However, the measured slope values and the existence of a linear region shows that in general, Taylor's equation is a good prediction of dispersion even in a turbulent jet.

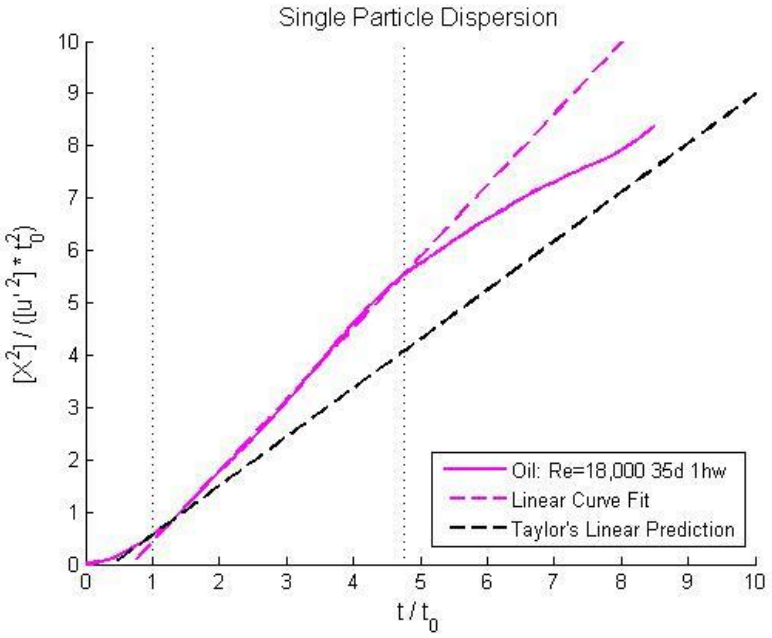

Figure 33: Linear fit for single particle dispersion as a function of time. Comparison of experimental data with Taylor's theoretical model.

Table 4: Ratio of experimental to theoretical linear fit coefficient

	Air	Oil
20d, 1hw	2.07	1.77
20d, 1.5hw	2.14	1.51
20d, 2hw	1.47	1.00
35d, 1hw	1.35	1.61
35d, 1.5hw	1.45	0.81

5.2 Pair Dispersion

The results of the pair dispersion experiments were analyzed using Batchelor's theory for tracer particle dispersion in homogeneous isotropic turbulence as a baseline. Although the conditions in these experiments were anything but homogeneous isotropic, with the shear rate and the turbulent dissipation rates varying widely across the jet, and the particles were lighter than the carrier fluid, this provides a clearly defined bar against which to compare these experimental dataset. The comparison of

the pair dispersion, non-dimensionalized with Batchelor's theoretical values, can be seen in Figure 34 for all five injection locations and Reynolds numbers in the experiments. The results show that the dispersion is initially much higher than the predicted value, and settles towards the same trend as Batchelor's theory for values of non-dimensional time (using the initial eddy turn-over time) of order one. After that time, the dispersion behaves exactly as Batchelor's prediction but with a factor of 1/3, that must be analyzed in more detail for the characteristics of the turbulence in the jet. The asymptotic time-square tendency predicted by Batchelor is reached more quickly by the oil droplets than by the air bubbles. It is important to note that Batchelor's prediction of the time-square evolution of the pair dispersion was determined on theoretical basis [2], and has been observed in experiments in homogeneous isotropic turbulence [6], for short times – comparable to the turn-over time of an eddy in the inertial range whose size is based on the initial separation of the particle pair. In that sense, the result in the experiments is counter to the theory, as the dispersion behavior is observed to evolve quadratically with time for times ***larger*** than the initial eddy turn-over time. This important discrepancy must be investigated to identify whether this is caused by the mean shear and inhomogeneity of the turbulence, or the buoyant character of the particles.

The results of pair dispersion for particles injected at 20 diameters from the nozzle and one half-width (Figure 34a) collapse well onto a single line. However, this consistency in the behavior of air bubbles and oil droplets for different Reynolds numbers decreases with distance from the nozzle. The results for 35 d and 1 half-width, and those for 20 d and 1.5 half-width injections are also quite uniform across experiments, while the results for the injections at 20 d and 2 half-widths and at 35 d and 1.5 half-widths present the most differences between experiments for different Re and particle types. This can be explained if one considers that the particles injected at 20 diameters and one half width are subjected to conditions that most closely resemble homogeneous isotropic turbulence, since they are in the region of the jet where the turbulence dissipation rate is highest and the mean shear is lower than other locations. Thus, the dispersion behavior can be modeled more closely by Batchelor's theory.

It is also observed that, in those the cases that produce a wide spread of the data after non-dimensionalization with Batchelor's model, the oil droplets converge to the t-square behavior more quickly than the air bubbles. A possible reason for this tendency is that the oil droplets are much closer to being neutrally buoyant, and are slightly smaller, than the air bubbles. These factors would cause the oil droplets to act more like tracer particles, and therefore respond more similarly to the fluid particles for which Batchelor developed his theoretical result.

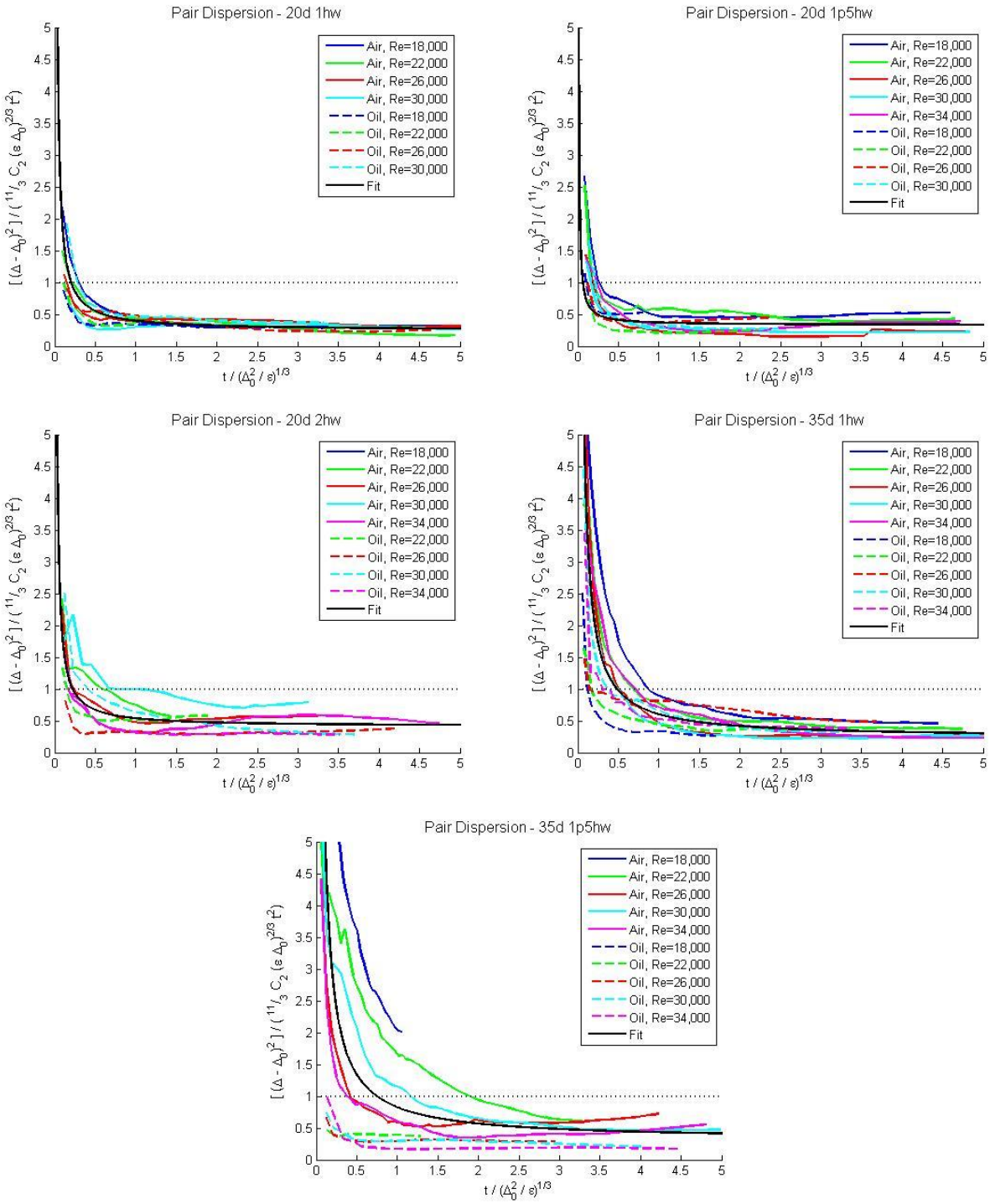

Figure 34: Comparison of data to Batchelor's equation

Carrying out the experiments in a turbulent jet resulted in an overall decrease in the asymptotic trend of pair dispersion, which the model from Batchelor must be adjusted to represent. A better fit to the long-

time trend of the data was achieved by multiplying Batchelor's equation by a factor of 1/3, resulting in the curves shown in Figure 35. Although these fits provide a better prediction of the dispersion data, there are still some wide discrepancies between the cases. Further analysis is needed to study the dependency of the pair dispersion on mean shear and turbulent dissipation rate inhomogeneity, well as on the particle inertia and terminal velocity. It may be possible to modify Batchelor's theory for the different turbulent conditions present in a jet, as well as for the different types of particles. Although these experiments have confirmed that Batchelor's theory does not perfectly predict pair dispersion in a turbulent round jet, the results show that there exists a similar quadratic relationship with time and a dependency on the turbulence dissipation rate of the flow.

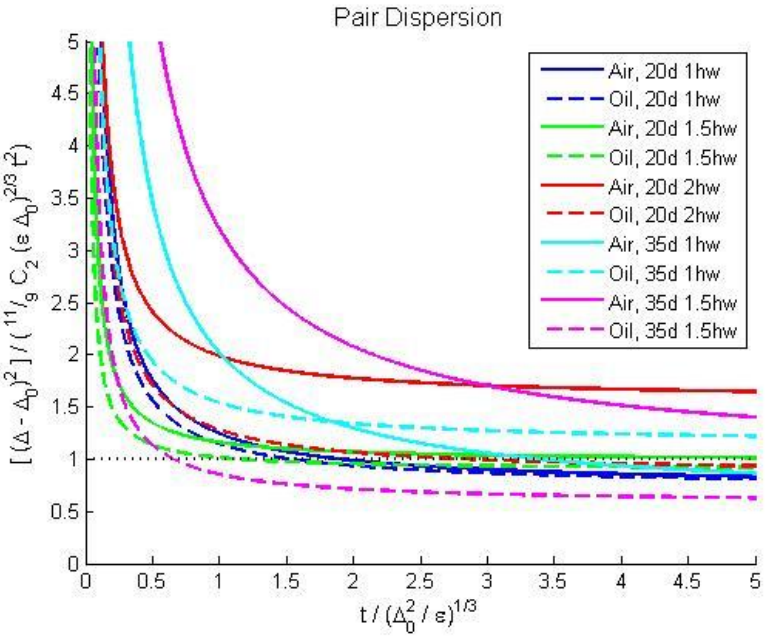

Figure 35: Comparison of data to adjusted Batchelor equation

5.3 Conclusions

This study, which compared the dispersion of particles against the simplified theories put forth by Taylor and Batchelor for homogeneous isotropic turbulence, examined a wide range of parameters to determine how they affected the scaling based on turbulence scales, dissipation rate and shear rate to predict particle dispersion. Although the study provided good insights into the relationships between these parameters, further examination is needed to better understand their effects. It is therefore

recommended that for future study, experiments with tracer particles in free shear turbulent flows and with buoyant particles in homogeneous isotropic turbulence be conducted and compared with the results presented here. This three way comparison will help isolate the dependency of turbulence and particle characteristics on dispersion so that the scaling can be adjusted and better predictive models can be developed for this complex, and more realistic, conditions.

References

[1] G. Taylor, "Diffusion by Continuous Movements," *Proc. London Math Soc.,* pp. 196-211, 1921.

[2] G. Batchelor, "The application of the similarity theory of turbulence to atmospheric diffusion," *Quarterly Journal of the Royal Meterological Society,* vol. 76, no. 328, pp. 133-146, 1950.

[3] L. F. Richardson, "Atmospheric Diffusion on a Distance-Neighbor Graph," *The Royal Society of London,* vol. 110, no. 756, pp. 709-737, 1926.

[4] W. S. a. J. Lumley, "Some Measurements of Particle Velocity Autocorrelation Functions in a Turbulent Flow," *J. Fluid Mech.,* vol. 48, pp. 41-71, 1971.

[5] M. W. a. D. Stock, "The effects of crossing trajectories on the dispersion of particles in a turbulent flow," *J. Fluid Mech.,* vol. 136, pp. 31-62, 1983.

[6] N. T. O. H. X. J. B. a. E. B. Mickael Bourgoin, "The Role of Pair Dispersion in Turbulent Flow," *Science,* vol. 311, pp. 835-838, 2006.

[7] J. P. a. P. Marie-Caroline Jullien, "Richardson Pair Dispersion in Two-Dimensional Turbulence," *Physical Review Letters,* vol. 82, no. 14, pp. 2872-2875, 1999.

[8] H. X. a. E. B. M. Gibert, "Inertial Effects on Two-Particle Relative Dispersion in Turbulent Flows," *EPL,* vol. 90, no. 64005, pp. 1-6, 2010.

[9] S. B. Pope, Turbulent Flows, New York: Cambridge University Press, 2000.

[10] S. P. C. a. W. K. G. Hussein J. Hussein, "Velocity Measurements in a high-Reynolds-number, momentum-conserving, axisymmetric, turbulent jet," *J. Fluid Mech.,* vol. 258, pp. 31-75, 1994.

[11] A. M. H. a. V. Ramjee, "Effects of the Axisymmetric Contraction Shape on Incompressible Turbulent Flow," *Journal of Fluid Engineering,* vol. 98, no. 1, pp. 58-68, 1976.